Cloud-Powered Flood Mapping and Impact Assessment: Leveraging Sentinel-1 SAR Imagery for Thailand's Disaster Response

Anucharn, T.,[1] Chaikaew, N.,[2] Sriprom T.[2] and Iamchuen N.[2*]
[1]Information Technology, School of Information and Communication Technology, University of Phayao, Phayao, Thailand
[2]Geographic Information Science, School of Information and Communication Technology, University of Phayao, Phayao, Thailand, E-mail: niti.ia@up.ac.th*
**Corresponding Author*

DOI: https://doi.org/10.52939/ijg.v21i5.4165

Abstract
This research presents a cloud-based application approach to flood mapping and impact assessment in Thailand, integrating Sentinel-1 Synthetic Aperture Radar (SAR) imagery with Google Earth Engine's computational capabilities. The study addresses the critical challenge of automated flood monitoring in Thailand's increasingly flood-prone landscape, where climate change and urbanization intensify disaster risks. The methodology combines multiple resolution geospatial datasets through a sophisticated processing framework that integrates dual-polarization SAR data analysis, advanced speckle reduction techniques, and topographic constraints. The system employs a robust change detection algorithm with a calibrated threshold value of 1.30, enhanced by permanent water body masking and connectivity analysis. The methodology was validated through case studies in five geographically diverse provinces: Chiang Rai, Phra Nakhon Si Ayutthaya, Nong Khai, Kanchanaburi, and Pattani. For instance, the Chiang Rai case study revealed 19,788 square kilometers of flooded area, impacting 6,392 residents and 16,795 buildings. The analysis highlighted differential vulnerability patterns, with agricultural areas experiencing a higher impact (5.41%) compared to urban zones (1.23%). This case study achieved an overall accuracy of 95.90% and a kappa coefficient of 0.92. Across all provinces, the system demonstrated exceptional performance with an average accuracy of 94.53% and an average kappa coefficient of 0.89. The cloud-based architecture facilitates efficient processing of large-scale datasets while maintaining high analytical precision. This capability makes the system an invaluable tool for emergency response and resource allocation. By providing timely and accurate flood metrics through an interactive web-based platform, this research significantly advances Thailand's flood monitoring capabilities, providing decision-makers with timely, accurate information for enhanced disaster management and response planning.

Keywords: Cloud Computing, Disaster Response, Flood Monitoring, Google Earth Engine, Sentinel-1 SAR

1. Introduction

Flooding represents one of the most devastating natural disasters globally, causing widespread human displacement, substantial economic losses, and severe environmental degradation. In Thailand, these challenges are particularly acute, with flooding events becoming increasingly frequent and severe due to climate change and rapid urbanization. The economic impact extends beyond immediate infrastructure damage, affecting agricultural productivity, industrial operations, and community resilience. Understanding and managing these flood events has become crucial for sustainable development and community safety in Thailand. The current situation in Thailand exemplifies the urgency of addressing flood-related challenges. Since mid-August 2024, various regions have experienced intensifying flood conditions [1], with the Department of Disaster Prevention and Mitigation (DDPM) reporting persistent difficulties in managing floodwaters due to continuous rainfall, particularly in the northern and northeastern regions [2]. Traditional flood monitoring and response systems often struggle to provide timely, accurate information necessary for effective disaster management.

Without implementing advanced technological solutions, communities remain vulnerable to flood impacts, potentially leading to increased loss of life, property damage, and economic disruption. The Thai Meteorological Department (TMD)'s predictions of changing climate patterns and increased rainfall further underscore the critical need for improved flood management strategies [3].

Sentinel-1 has emerged as a powerful tool for flood monitoring and addressing various remote sensing challenges. Initially consisting of two satellites, Sentinel-1A and Sentinel-1B, the mission was designed to work in tandem to enhance temporal resolution. However, Sentinel-1B experienced a malfunction in December 2021, reducing the constellation's coverage capacity [4]. The Synthetic Aperture Radar (SAR) instrument on Sentinel-1 operates at C-band, offering high reliability, improved revisit time, geographical coverage, and rapid data dissemination. These capabilities support operational applications in marine monitoring, land monitoring, emergency services, climate change, and security [5]. One of the key features of Sentinel-1 SAR data is its all-weather imaging capability, which allows it to penetrate clouds and operate in darkness [6]. The mission provides global coverage with a repeat cycle of 12 days (175 orbits) for a single satellite, or a 6-day repeat cycle when both Sentinel-1A and Sentinel-1B are operating in ascending and descending orbits [5] and [7]. Sentinel-1's SAR system operates in four distinct imaging modes, each optimized for specific applications through unique combinations of coverage and resolution [8].

The interferometric wide swath (IW) mode operates as the principal imaging configuration for Sentinel-1's land-based applications, offering dual-polarization capabilities through two distinct transmission/reception combinations. The first configuration pairs single co-polarization using vertical transmit/vertical receive (VV) with dual-band cross-polarization via vertical transmit/horizontal receive (VH). The second configuration employs single co-polarization with horizontal transmit/horizontal receive (HH) alongside dual-band cross-polarization using horizontal transmit/vertical receive (HV). This dual-polarization design provides flexibility in capturing surface characteristics, where co-polarized channels (VV or HH) enhance sensitivity to geometric structures like buildings or vegetation, while cross-polarized channels (VH or HV) improve detection of volumetric scattering in complex terrains such as forests or floodplains. The IW mode's swath width of 250 km and 5 m × 20 m spatial resolution make it particularly suited for large-scale environmental monitoring tasks requiring both broad coverage and detailed polarization information [9]. Extra wide swath (EW) mode expands coverage to 400 km for maritime and polar monitoring, while Stripmap (SM) mode provides 80 km swaths at 5 m resolution for compatibility with legacy missions like ERS and Envisat [10]. Both IW and SM support single (HH/VV) or dual polarization configurations. The wave mode (WV), designed for oceanographic studies, captures 20 km x 20 km vignettes at 100 km intervals using single polarization (HH or VV) [11]. As the default mode over open oceans, WV continues the observational legacy of earlier missions but with enhanced spatial resolution. These modes operate exclusively, with IW and WV handling routine land and ocean observations respectively, while EW and SM address specialized requirements like sea-ice monitoring or emergency response [12].

Google Earth Engine (GEE) has emerged as a game-changing complement to Sentinel-1's capabilities, revolutionizing environmental monitoring and analysis through its cloud-based geospatial processing platform. At the heart of GEE's power lies its vast catalog of remotely sensed datasets, a treasure trove of over 600 petabytes of satellite imagery and geospatial data stretching back to the 1970s [13]. This immense data repository, when coupled with GEE's formidable cloud computing prowess, unlocks the potential for efficient processing and analysis of large-scale geospatial data across a myriad of applications. The GEE data catalog is a veritable cornucopia of information, encompassing an impressive array of datasets. From satellite imagery captured by various sensors to climate and weather data, from land cover and land use products to digital elevation models, and even socioeconomic datasets, GEE offers a comprehensive suite of geospatial information. This wealth of data, combined with the platform's ability to process and analyze massive amounts of geospatial information in near real-time using the intuitive Earth Engine Code Editor [14], has ushered in a new era of informed decision-making. Whether it's natural resource management, environmental monitoring, or disaster response, GEE has become an indispensable tool for professionals and researchers alike, enabling them to make more timely and accurate decisions based on up-to-date geospatial insights [15].

While flood inundation detection using SAR imagery combined with GEE is a well-established approach, this study introduces a significant advancement by integrating these technologies into a web-based platform for real-time flood impact assessment.

The novelty of this research lies in its comprehensive web-based interface, which seamlessly integrates Sentinel-1 SAR data analysis with GEE's computational capabilities to provide timely and accurate flood metrics. This platform allows users to interactively explore flood extent and impact analysis results, offering detailed insights into population exposure, infrastructure damage, and agricultural impacts [16]. By making these critical insights accessible through a user-friendly web interface, this study enhances decision-making capabilities for emergency responders and policymakers, providing a scalable framework that can be adapted to other regions facing similar flooding challenges. The web-based presentation of results facilitates broader accessibility and usability, enabling stakeholders to quickly assess flood impacts and develop targeted response strategies.

The significance of this research extends to various stakeholders: emergency responders gain access to timely, accurate flood information for improved response coordination; local authorities benefit from enhanced decision-making capabilities for resource allocation and evacuation planning; and communities receive better risk assessment information. Furthermore, the system's scalable nature makes it adaptable to other regions facing similar flooding challenges. The study's objectives are threefold: first, to design and develop an automated script suite on the GEE platform for enhancing rapid flood mapping and impact assessment processes using Sentinel-1 SAR data, building upon the UN-SPIDER methodology framework [17]; second, to demonstrate the potential of cloud-based geospatial analysis for disaster response and decision support; and finally, to evaluate and validate the accuracy of the flood mapping and impact assessment system through comparison with authoritative data from reputable agencies. While satellite imagery cannot always provide real-time flood data due to factors like satellite revisit times and data processing delays, this system offers a rapid and efficient approach to flood mapping. By leveraging Sentinel-1 SAR data and GEE's computational capabilities, the system can process large datasets quickly, providing critical insights into flood extent and impact shortly after data becomes available. This capability is crucial for emergency responders and policymakers who require timely information to coordinate effective disaster responses.

This research stands out by combining Sentinel-1 SAR data with the processing power of GEE to create a high-accuracy flood mapping system that can be adapted to Thailand's diverse geography. The system utilizes pre- and post-flood satellite imagery to accurately delineate disaster-affected areas through advanced temporal analysis, enabling clear identification of inundated zones. The system employs advanced change detection techniques, utilizing a tailored threshold value, and filters out areas with high slopes and those with fewer than eight connected pixels to reduce false positives and enhance flood area identification accuracy. Additionally, integrating JRC Global Surface Water data effectively distinguishes between flooded areas and permanent water bodies, allowing the system to provide comprehensive and accurate information on flood extents and impacts on agricultural and urban areas. This research aims to develop a precise and adaptable flood mapping system for Thailand, which will enable disaster response units to plan and execute their operations more efficiently.

GEE facilitates economic loss estimation, particularly in agriculture and communities sectors disproportionately impacted by floods providing critical data for targeted recovery planning. The cloud-based architecture of GEE eliminates the need for high-performance computing infrastructure, allowing disaster response units even in remote areas to access and process data efficiently. This accessibility ensures operational readiness regardless of technical expertise in geospatial analysis. Designed for nationwide scalability, the system’s flexibility enables adaptation to diverse regional hydrological conditions across Thailand, from floodplains to urban-industrial zones. Its integration with multi-source datasets supports dynamic decision-making for resource allocation, evacuation planning, and post-disaster damage assessment. This research addresses the critical need for improved flood management in Thailand. Building on previous work in flood mapping [18][19][20][21] and [22], agricultural monitoring [23] and [24], and urban growth assessment [25] and [26]. The developed system utilizes GEE's serverless architecture to bypass traditional requirements for localized data storage and manual preprocessing [27], while establishing a unified geospatial platform that automates flood monitoring workflows through several technical advancements.

2. Research Methodology

The conceptual framework illustrated in Figure 1 provides a detailed workflow for flood mapping and impact assessment using Sentinel-1 SAR imagery and GEE. The process begins with the selection of provincial boundaries and the specification of pre-flood and post-flood periods. These temporal parameters are critical for identifying changes in flood conditions over time.

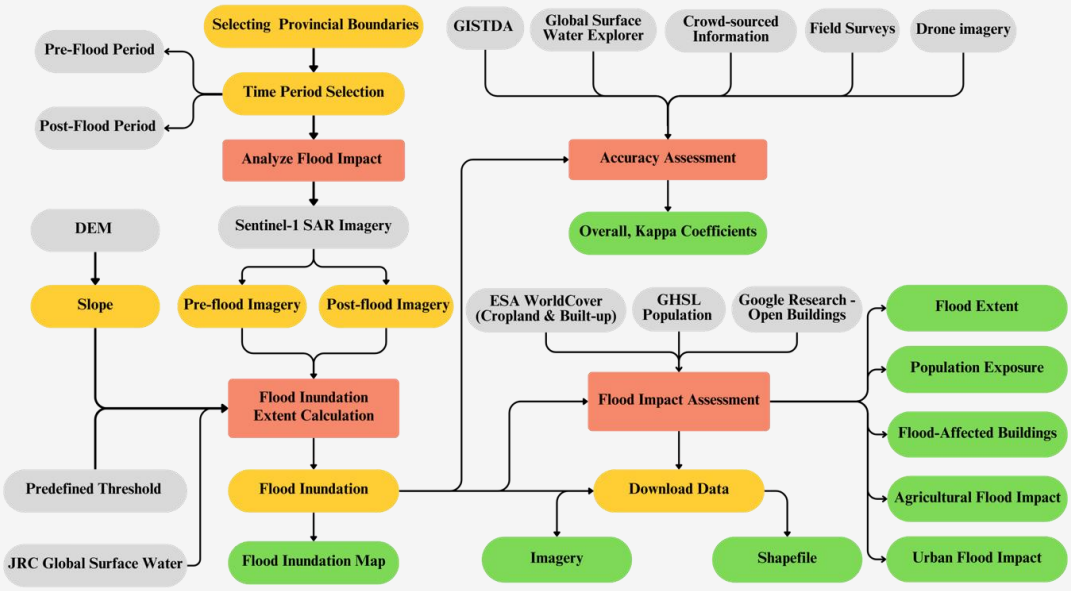

Figure 1: Conceptual framework of cloud-powered flood mapping and impact assessment

Digital Elevation Model (DEM) data is then incorporated to analyze slope characteristics, which are essential for refining flood inundation calculations. Sentinel-1 SAR imagery is processed to extract pre-flood and post-flood images, enabling the calculation of flood inundation extent through change detection techniques. This step involves applying a predefined threshold value and integrating JRC Global Surface Water data to distinguish between permanent water bodies and floodwaters. The result is a flood inundation map that highlights affected areas.

The next phase focuses on assessing the impact of flooding. Using datasets such as ESA WorldCover for land cover classification, GHSL population data for demographic analysis, and building footprint data from Google Research, the system evaluates flood impacts across several dimensions: flood extent, population exposure, affected buildings, agricultural damage, and urban area impacts. These metrics are calculated by overlaying the flood inundation map with respective geospatial datasets.

The accuracy validation process employs a multi-source verification approach, comparing generated flood extent maps against authoritative references including: 1) Geo-Informatics and Space Technology Development Agency (GISTDA) flood monitoring data (https://disaster.gistda.or.th/flood/), 2) the European Commission's Global Surface Water Explorer (https://global-surface-water.appspot.com /map), 3) high-resolution drone imagery, 4) field survey observations, and 5) ground-truth information from local communities. This comprehensive validation framework calculates quantitative performance metrics including overall classification accuracy and Cohen's kappa coefficients to statistically confirm the flood mapping reliability.

Finally, the results are visualized through a web-based dashboard that integrates spatial data layers for detailed analysis. This dashboard allows users to toggle between layers representing different impact categories, facilitating a comprehensive understanding of flood effects. The system also supports data export in various formats (e.g., imagery and shapefiles), enabling further analysis in external Geographic Information System (GIS) platforms.

The methodology framework consists of five main components, each designed to address specific research objectives. These components are described as follows:

2.1 Study Area

The study focuses on Thailand's 77 provinces, categorized into six main regions based primarily on geographical characteristics, supplemented by factors such as climate conditions, cultural dimensions, ethnic diversity, linguistic variations and local lifestyles [28]. These six regions include the Northern, Northeastern, Central, Eastern, Western, and Southern regions (Figure 2). This comprehensive framework integrates physical factors with flood mapping techniques using Sentinel-1 SAR satellite imagery to establish an efficient flood boundary analysis system.

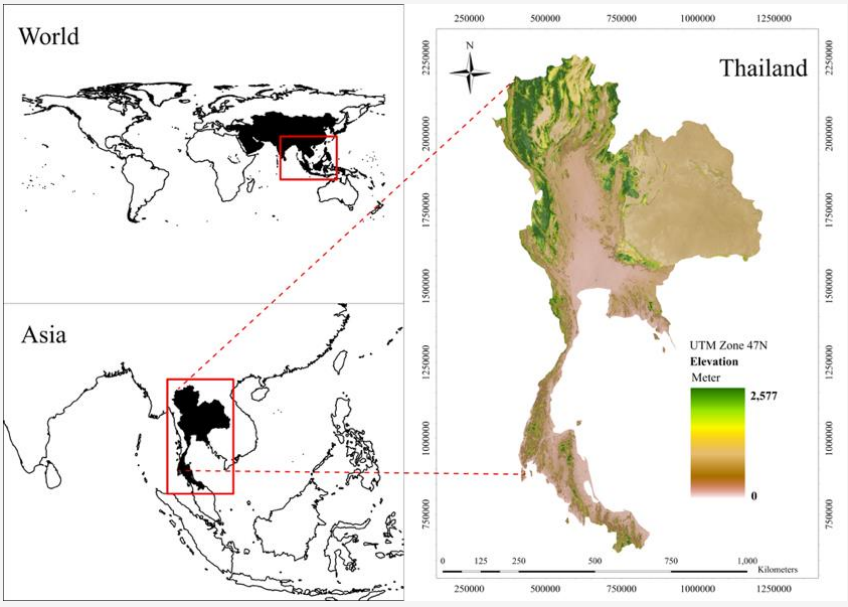

Figure 2: Map of study area in Thailand

It enables retrospective analysis of major flood events, such as the 2024 floods across multiple Thai provinces: Chiang Rai (Northern region), Phra Nakhon Si Ayutthaya (Central region), Nong Khai (Northeastern region), Kanchanaburi (Western region), and Pattani (Southern region). The system employs GEE for spatial data integration, offering an intuitive interface that allows users to select specific provinces and time periods to visualize flood boundaries and automatically assess flood impacts according to their requirements.

For validation purposes, the study selected five representative provinces from each region, cross-verifying flood boundary determinations with multiple data sources from GISTDA, global surface water explorer, drone imagery, field surveys, and crowd-sourced information. This multi-source validation approach ensures system reliability and establishes its suitability for extrapolation to flood boundary delineation across all 77 Thai provinces. The methodology aligns with international validation standards specified in the EU Floods Directive, which recommends using 3-5 representative areas per country when regions demonstrate hydrological homogeneity [29].

2.2 Data Collection

The methodology for flood mapping and impact assessment relies on a diverse set of geospatial datasets, each contributing essential information for analysis. The data collection process is divided into two categories: primary data sources and supporting datasets.

2.2.1 Primary data source

The Sentinel-1 SAR imagery serves as a critical dataset for flood monitoring, leveraging its unique capacity to operate effectively in all weather conditions and at any time of day. This capability is particularly advantageous during heavy rainfall events, when optical sensors are rendered ineffective due to cloud cover [30]. The Level-1 Ground Range Detected (GRD) dataset [31], processed through the Sentinel-1 Toolbox, contains focused SAR data that undergoes detection, multi-looking, and ground-range projection using the WGS84 Earth ellipsoid model [30]. Since its operational launch in October 2014, the GRD dataset has been updated daily, with new acquisitions integrated into processing systems within two days, enabling near-real-time disaster response capabilities critical for flood emergencies [32].

The GRD processing chain involves radiometric calibration to backscatter coefficients (σ^o or γ^o), thermal noise removal, optional speckle filtering to reduce image noise, and orthorectification using Range-Doppler terrain correction paired with DEM [33] and [34]. These steps ensure both geometric precision and radiometric accuracy, making the data suitable for diverse applications such as crop monitoring, land-use change detection, and detailed flood impact assessments. In this case, the final product features square spatial resolution pixels (10 m × 10 m) with reduced speckle noise [35] and [36].

The IW mode is especially valuable for flood mapping, providing broad coverage and dual-polarization capabilities (VV/VH) that enhance water detection in complex environments like urban areas or vegetated floodplains [37].

Dual-polarization data provides critical flexibility: VH polarization reduces backscatter uniformly across flooded landscapes, simplifying differentiation between water and land, especially in densely vegetated zones [37]. Conversely, VV polarization's sensitivity to vertical structures aids in detecting flooded urban areas with emergent vegetation or buildings, though it may exhibit increased backscatter due to double-bounce effects [17][38] and [39]. Threshold-based methods are widely employed for instantaneous flood detection [40], leveraging low backscatter signatures in normally dry areas to identify inundation zones [41]. Platforms like GEE streamline large-scale analysis by integrating SAR data with auxiliary datasets (e.g., DEMs, population grids) to map flood extents and assess impacted populations rapidly [42].

2.2.2 Supporting datasets

To complement the Sentinel-1 SAR data, several supporting datasets are integrated into the analysis framework:

1) Administrative Boundaries [43]: Provincial boundaries from FAO/GAUL/2015 are used to define the study area and facilitate spatial analysis at the provincial level.

2) Digital Elevation Data [44]: NASA's shuttle radar topography mission (SRTM) provides elevation data at a resolution of 30 meters. This dataset is used for terrain analysis, including slope calculations, which help refine flood extent mapping by excluding areas unlikely to experience flooding due to steep gradients.

3) Surface Water Data [45]: The JRC global surface water mapping layers offer insights into water seasonality and permanent water bodies. This dataset helps distinguish between floodwaters and existing water bodies, ensuring accurate delineation of inundated areas.

4) Land Cover Information [46]: ESA WorldCover provides land cover classification at a resolution of 10 meters. Specific focus is given to cropland (class value 40) and built-up areas (class value 50), which are essential for assessing agricultural and urban impacts of flooding.

5) Population Data [47]: The Global Human Settlement Layer (GHSL) provides population count and built-up surface data at a resolution of 100 meters. This dataset enables demographic analysis to estimate population exposure in flood-affected areas.

6) Infrastructure Data [48]: Microsoft Building Footprints for Thailand, available in GeoJSON format, provide detailed information on building locations and structures within the study area. This dataset supports infrastructure impact assessment by quantifying affected buildings.

These datasets are accessed through GEE (Table 1), which serves as the central platform for data processing and analysis. GEE's computational capabilities allow efficient handling of large-scale geospatial datasets, enabling rapid generation of flood maps and impact metrics. Each dataset contributes unique attributes that enhance the accuracy and comprehensiveness of the flood mapping methodology, making this approach adaptable to diverse geographical contexts.

2.3 Data Analysis

The data analysis workflow comprises three crucial stages: data preprocessing, flood inundation extent calculation, and impact assessment. Each stage leverages advanced spatial analysis techniques through GIS to generate comprehensive impact metrics. This methodology enables a deep understanding of flood impacts across economic, social, and environmental dimensions. The resulting insights serve as a valuable tool for executives and stakeholders to effectively plan disaster responses in flood-prone areas.

2.3.1 Data preprocessing

Data preprocessing is a crucial step in preparing Sentinel-1 SAR imagery for flood analysis and mapping. This process comprises three main stages: data selection and filtering, temporal data processing, and speckle noise reduction. All these operations are performed on the Google Earth Engine platform to ensure processing efficiency and consistency.

The initial stage begins with careful data selection from the Sentinel-1 GRD collection, focusing on images acquired in IW mode with VH polarization. This combination provides optimal sensitivity for water surface detection [49]. The spatial resolution is maintained at 10 meters to preserve detailed surface features while ensuring manageable computational requirements.

The temporal data processing stage involves collecting imagery from two distinct periods - pre and post the flood event. This temporal selection is crucial for the change detection approach used in flood mapping. The system automatically verifies data availability within the specified timeframes to ensure sufficient coverage for analysis. When multiple images are available within each period, they are processed to create a comprehensive mosaic, which is then precisely clipped to the study area boundaries to optimize processing efficiency. The final stage addresses speckle noise reduction, a characteristic feature of SAR imagery, to enhance image quality. This step employs a spatial filtering technique, utilizing a focal mean filter with a smoothing radius of 50 meters using a circular kernel [50]. The circular kernel is specifically chosen to ensure uniform smoothing in all directions, preserving the spatial patterns of flooding while reducing noise artifacts. This filtering process is applied consistently to both pre-flood and post-flood imagery to maintain comparative analysis integrity. The use of an appropriate radius ensures effective noise reduction without causing excessive blurring.

Table 1: Datasets and specifications used in the study

Datasets	Earth Engine Snippet	Band		Resolution (Meter)	URL
		Name	Description		
Sentinel-1 SAR GRD	ee.ImageCollection("COPERNICUS/S1_GRD")	VH	Dual-band cross-polarization, vertical transmit/horizontal receive	10	https://developers.google.com/earth-engine/datasets/catalog/COPERNICUS_S1_GRD
Province Boundaries	ee.FeatureCollection("FAO/GAUL/2015/level1")	ADM0_NAME	UN country name		https://developers.google.com/earth-engine/datasets/catalog/FAO_GAUL_2015_level1
NASA SRTM Digital Elevation	ee.Image('USGS/SRTMGL1_003')	elevation	Elevation	30	https://developers.google.com/earth-engine/datasets/catalog/USGS_SRTMGL1_003
JRC Global Surface Water Mapping Layers	ee.Image('JRC/GSW1_4/GlobalSurfaceWater')	seasonality	Number of months water is present		https://developers.google.com/earth-engine/datasets/catalog/JRC_GSW1_4_GlobalSurfaceWater
ESA WorldCover	ee.ImageCollection("ESA/WorldCover/v100")	Map	Landcover class value of 40 represents Cropland and 50 represents Built-up	10	https://developers.google.com/earth-engine/datasets/catalog/ESA_WorldCover_v100
GHSL: Global population surfaces	ee.ImageCollection("JRC/GHSL/P2023A/GHS_POP")	population_count	Population count by epoch	100	https://developers.google.com/earth-engine/datasets/catalog/JRC_GHSL_P2023A_GHS_POP
Google Research - Open Buildings	ee.FeatureCollection("GOOGLE/Research/open-buildings/v3/polygons")	Open Buildings V3 Polygons	GeoJSON format		https://developers.google.com/earth-engine/datasets/catalog/GOOGLE_Research_open-buildings_v3_polygons

However, using too large a radius can lead to over-smoothing, potentially losing fine details in areas with complex terrain or mixed land use. This issue highlights the importance of selecting the right filter parameters to balance noise reduction and detail preservation. Over-smoothing can result in the loss of critical information, especially in regions with diverse land cover or topography, which are common in flood-prone areas [51] and [52].

The entire preprocessing workflow is designed to be automated and efficient, leveraging GEE's cloud computing capabilities. This approach not only ensures processing consistency but also enables rapid analysis of large areas, making it particularly valuable for time-critical flood monitoring applications. The resulting preprocessed imagery provides a robust foundation for subsequent flood extent mapping and impact assessment analyses.

2.3.2 Flood inundation extent calculation

The methodology initiates with the careful selection of pre-flood and post-flood Sentinel-1 SAR imagery. A change detection approach is implemented to isolate areas exhibiting significant alterations in surface characteristics attributable to flooding events. Central to this process is the computation of the backscatter ratio (*BR*), defined as the post-flood backscatter coefficient (σ^0_{post}) divided by the pre-flood backscatter coefficient (σ^0_{pre}) as presented in Equation 1:

$$BR = \frac{\sigma^0_{post}}{\sigma^0_{pre}}$$

Equation 1

This ratio-based methodology, enhances flood detection accuracy by emphasizing relative changes in surface water conditions while mitigating residual effects of terrain geometry and radar calibration inconsistencies. Elevated ratio values (bright pixels) indicate substantial reductions in backscatter intensity, typically associated with newly inundated areas, whereas lower values (dark pixels) correspond to minimal changes, effectively distinguishing permanent water bodies from transient floodwaters.

The technique demonstrates superior performance over single-image thresholding methods by intrinsically filtering regions with inherent low backscatter characteristics, such as smooth asphalt surfaces or calm water bodies, through its differential analysis framework [53][54] and [55]. By focusing on temporal changes rather than absolute backscatter values, the approach minimizes false positives and improves flood boundary delineation, particularly in complex landscapes. The resultant difference imagery provides a spatially explicit representation of flood extent, validated through alignment with UN-SPIDER's operational flood mapping protocols.

The selection of an optimal threshold value is critical for accurately classifying flooded and non-flooded areas in SAR-based flood mapping. This threshold determines the minimum ratio between post-flood and pre-flood backscatter values required to identify inundation. When water inundates dry land, the resulting change in surface characteristics typically generates a pronounced increase in this ratio. The chosen threshold directly influences the trade-off between false positives (misclassified dry areas) and false negatives (undetected flood zones). The validation process utilized a confusion matrix framework to evaluate flood detection accuracy, leveraging threshold values derived from the GISTDA flood monitoring system. For the September 6, 2024, Chiang Rai flood event, 512 randomly sampled validation points were extracted from GISTDA's flood-affected area maps. Threshold values ranging from 1.20 to 1.40 were systematically tested, revealing significant performance variations in flood extent mapping, as summarized in Table 2.

The 1.30 threshold emerged as the most effective, achieving 95.90% classification accuracy when validated against data from Chiang Rai. This high accuracy underscores its robustness in distinguishing flooded areas from dry regions. In contrast, the 1.20 threshold performed poorly, with an accuracy of 79.10%, indicating its unreliability for practical flood detection. The optimization process demonstrated that the 1.30 threshold optimally balances sensitivity (ability to correctly identify flooded zones) and specificity (ability to exclude non-flooded areas), making it the preferred choice for accurate flood monitoring.

Recent advancements in Synthetic Aperture Radar (SAR)-based flood mapping have demonstrated the critical role of threshold optimization, particularly highlighting the efficacy of a 1.30 threshold in operational flood detection systems. Empirical validation of the Change Detection and Thresholding (CDAT) method has revealed distinct polarization-dependent configurations for accurate flood characterization.

Table 2: Confusion matrix for determining the optimal flood threshold

Threshold	Correct		Incorrect		Overall Accuracy	Kappa Coefficient
	Flooded	Non-Flooded	Flooded	Non-Flooded		
1.20	157	248	8	99	79.10	0.58
1.25	164	324	1	23	95.31	0.90
1.30	237	254	2	19	95.90	0.92
1.35	151	272	14	75	82.62	0.64
1.40	137	281	28	66	81.64	0.60

For VH polarization, researchers identified 1.3 as the optimal coefficient for detecting open floodwaters, paired with 2.5 for identifying flooded vegetation. This combination effectively balances sensitivity to smooth water surfaces while minimizing false positives in areas with dense vegetation. In contrast, VV polarization requires finer calibration due to its inherent sensitivity to surface roughness and vertical structures. Here, a lower coefficient of 1.2 maximizes open floodwater detection accuracy, while 2.5 remains suitable for vegetated inundation. The adjustment reflects VV's heightened responsiveness to geometric interactions, such as double-bounce effects between water and upright vegetation a phenomenon less pronounced in VH [56]. The threshold application in Equation 2 is a binary classification rule used to delineate flooded areas from SAR-derived backscatter data. The equation is defined as:

$$\text{Flooded Area} = \begin{cases} 1, & \text{if Ratio} \geq 1.30 \\ 0, & \text{otherwise} \end{cases}$$

Equation 2

Here, 1 indicates a flooded pixel (backscatter ratio meets or exceeds the threshold), and 0 represents a non-flooded pixel (ratio below the threshold). A ratio ≥ 1.30 reflects a significant drop in backscatter intensity, typically caused by smooth water surfaces acting as specular reflectors, which deflect radar waves away from the sensor. This drop in backscatter reliably classifies the pixel as "flooded".

In SAR-based flood mapping, connectivity analysis is crucial for refining map accuracy by eliminating isolated pixels that may not represent actual flooding. After applying a threshold to identify potential flood areas, this technique examines each pixel's spatial relationship with its neighbors to determine if it is connected to other flooded pixels. Isolated pixels are considered noise and removed to improve accuracy. A common criterion requires a pixel to be connected to at least eight neighboring pixels, ensuring only significant clusters of flooded pixels are retained. This approach reduces false positives and enhances overall accuracy by mapping only contiguous flood areas. Connectivity analysis is often integrated with other techniques, such as topographic constraints using DEM and permanent water body masking, to further improve accuracy. Topographic constraints remove pixels on slopes greater than 5% where significant flooding is unlikely, while spatial connectivity analysis eliminates isolated pixels that might represent noise. This integrated approach ensures that the final maps are both precise and reliable, providing more reliable information for flood response and management efforts.

Lastly, the method for permanent water body masking utilizes the JRC global surface water mapping layers dataset [45]. This dataset provides insights into water seasonality and permanent water bodies, which is crucial for distinguishing between floodwaters and existing water bodies [57]. The JRC dataset is used to create a mask for permanent water bodies, where areas containing water for more than 10 months annually are classified as permanent features and excluded from flood extent calculations. This masking process is integrated into the flood mapping workflow by applying it to the change detection results, ensuring that only actual floodwaters are mapped. Additionally, refinement techniques such as spatial connectivity analysis and topographic constraints are applied to further enhance the accuracy of flood extent mapping by reducing false positives in areas unlikely to experience flooding.

The final step involves the quantification of the flood extent area. This calculation converts the binary flood mask into actual area measurements by multiplying each identified flood pixel by its ground surface area. The total flood extent is then computed by summing these areas across the entire region of interest, with the results converted from square meters to square kilometers. This comprehensive approach ensures accurate flood extent mapping while minimizing potential sources of error through multiple validation and refinement steps.

The process leverages GEE's computational capabilities to handle large-scale analyses efficiently, making it particularly valuable for rapid flood assessment and emergency response applications.

The resulting flood extent maps provide crucial information for disaster response teams and decision-makers, enabling them to quickly identify and prioritize affected areas for intervention.

2.3.3 Impact assessment

Prior to the calculation in the impact assessment phase, the flood extent data is adjusted to match the projection systems of the population data from GHSL, urban and agricultural areas from ESA WorldCover, and building data from Open Buildings. This alignment ensures spatial accuracy by maintaining consistent projections across datasets, allowing for precise evaluation of various impacts. The overlay process facilitates accurate assessment of different impacts. Subsequently, a reducer function is applied to compute the total affected area within the specified boundary. This step is crucial for obtaining comprehensive statistics on the extent of flooding and its impacts across multiple dimensions, such as population exposure, urban areas, agricultural lands, and infrastructure.

Population exposure analysis utilizes the GHSL data at a 100-meter resolution. This demographic assessment involves overlaying the flood extent mask with population count data, enabling precise estimation of affected populations within the inundated areas. The equation for calculating the exposed population (E_P) is defined in Equation 3:

$$E_P = \sum_{i=0}^{n} P_i F_i$$

Equation 3

Where P_i is the population in pixel i, F_i is binary flood mask indicating flooded pixel, and n is the total number of flooded pixel. The process involves multiplying the population count in each pixel by the flood mask to determine the total population exposed to flooding within the inundated areas. This approach provides accurate insights into the number of people affected by flooding, which is crucial for humanitarian response planning.

Agricultural impact evaluation leverages the ESA WorldCover dataset to identify and quantify affected cropland areas. The analysis specifically focuses on areas classified as cropland (class value 40) and calculates both the total agricultural area and the portion affected by flooding. These calculations are performed using pixel-based area computations and are converted to square kilometers for practical application. This detailed agricultural assessment provides essential information for agricultural damage estimation and recovery planning. The flood affected agricultural area (A_A) is determined from Equation 4:

$$A_A = \sum_{i=0}^{n} A_i C_i$$

Equation 4

Where A_i is the area of pixel i and C_i is a binary mask indicating if the pixel is classified as flooded cropland.

Urban impact assessment utilizes the ESA WorldCover data to identify affected urban regions, employing class value 50 to denote urban areas. The calculation of the affected urban area involves multiplying each pixel's area by its actual ground surface area. This step is crucial for obtaining comprehensive statistics on the extent of urban flooding. Finally, converting the area from square meters to square kilometers presents the results in a clear and meaningful format, which is highly beneficial for disaster response planning. The affected urban area (A_U) is determined from Equation 5:

$$A_U = \sum_{i=0}^{n} A_i U_i$$

Equation 5

Where A_i is the area of pixel i and U_i is a binary mask indicating if the pixel is classified as flooded urban.

Infrastructure impact quantification incorporates detailed building footprint data from Google Research - Open Buildings. This analysis involves converting vector building data to raster format, maintaining 10-meter resolution consistency with the flood extent mapping. The process includes spatial overlay analysis to identify affected structures, providing both total building counts and the number of buildings impacted by flooding within the study area. The flood affected buildings (A_B) is determined from Equation 6:

$$A_B = \sum_{i=0}^{n} B_i F_i$$

Equation 6

Where B_i is the number of buildings in pixel i and F_i is a binary mask indicating if the pixel is flooded.

2.4 Implementation Architecture and System Design

The implementation architecture leverages the powerful capabilities of GEE, employing JavaScript to create a sophisticated cloud-based geospatial analysis system.

This framework significantly enhances the efficiency of flood mapping and impact assessment workflows through several key technological and architectural decisions. The system architecture is specifically designed to process and analyze multi-temporal satellite imagery for flood detection and impact assessment.

The user interface emphasizes operational efficiency and intuitive interaction, incorporating sophisticated geospatial processing capabilities. The system facilitates seamless definition of spatial and temporal parameters through an interactive web-based interface. Users can delineate areas of interest (AOI) using administrative boundaries at the provincial level, supporting both single-province and multi-province analytical scenarios. The temporal analysis framework enables users to specify pre-flood and post-flood periods, facilitating change detection and impact assessment through multi-temporal satellite imagery analysis. Advanced processing parameters, including SAR polarization selection and threshold value optimization, can be fine-tuned to enhance flood detection accuracy.

The visualization module incorporates dynamic web mapping capabilities powered by the GEE API, enabling interactive exploration of flood extent and impact analysis results. The analytical engine generates comprehensive geospatial statistics, including flood area calculations, population exposure metrics derived from demographic datasets, building footprint impact assessments, and land use classification analysis for both urban and agricultural areas. The cloud-based processing architecture ensures efficient handling of large-scale geospatial datasets while maintaining high spatial resolution and analytical precision.

The system supports comprehensive data export functionality, allowing users to extract both raster imagery and vector shapefiles for integration with other GIS. The Earth Engine Code Editor serves as a web-based integrated development environment (IDE) for the Earth Engine JavaScript API, specifically designed to facilitate complex geospatial workflow development. This interface provides direct access to Google's extensive satellite imagery catalog, enabling sophisticated remote sensing analysis through an intuitive coding environment. The Code Editor's functionality streamlines the development of complex geospatial workflows, offering immediate visualization of results and efficient processing of large-scale Earth observation data.

2.5 Geospatial Accuracy Assessment Methodology Using Provincial Representatives in Thailand

The methodological framework for validating flood classification accuracy across Thailand employs a stratified sampling strategy that accounts for hydrological, topographical, and climatic variability. Five representative provinces were selected for this study Chiang Rai (Northern region), Phra Nakhon Si Ayutthaya (Central region), Nong Khai (Northeastern region), Kanchanaburi (Western region), and Pattani (Southern region) to ensure comprehensive validation across diverse geographical and land use characteristics.

The methodology employs random point sampling [58], evaluated using overall accuracy and kappa coefficient analysis, with careful consideration of statistical sample size determination to ensure robust validation results across Thailand's diverse geographical landscapes. The sampling design employed in this accuracy assessment follows established geospatial validation principles based on probability theory.

The determination of 256 random sampling points was derived using Equation 7, which is grounded in binomial probability distribution theory [59]. This statistical approach allows for the calculation of the minimum sample size required to achieve specific confidence levels and margins of error. The equation considers the desired level of overall map accuracy (80%) and an acceptable margin of error (5%), producing a statistically sound number of validation points that balance practicality with scientific rigor.

The application of binomial probability theory in this context acknowledges the binary nature of accuracy assessment, where each point is either correctly or incorrectly classified. The sample size determination equation can be expressed in Equation 7:

$$N = \frac{Z^2 pq}{E^2}$$

Equation 7

Where N represents the required sample size, Z is the standard normal deviate (1.96 for 95% confidence level), p is the expected proportion of accuracy (0.8 in this study), q is the complement of the expected accuracy percentage (100 - p) and E is the allowable error (0.05).

The application of random point sampling, guided by systematic design principles, aims to ensure unbiased representation of the five selected provinces.

This random sampling was performed using geographic software that generated points according to random sampling protocols. This method guarantees that every location within the study area has an equal chance of being selected, thereby eliminating sampling biases that could impact the accuracy of assessments.

In the study, 256 sampled points are allocated among the provinces affected by flooding, with the distribution proportional to the relative areas of the five provinces. Additionally, another 256 points are used for non-flooded areas, resulting in a total of 512 points. This approach ensures a balanced representation of both flooded and non-flooded regions, allowing for a comprehensive analysis of the flood dynamics across different provinces. Moreover, using an equal number of points for both flooded and non-flooded areas allows for a direct comparison between these two conditions, facilitating the identification of distinct patterns and characteristics that differentiate flooded from non-flooded regions. This balanced approach supports the development of more accurate models and enhances the reliability of the findings, as it provides a comprehensive view of the flood scenario and its impacts on different areas.

This study employs a comprehensive validation methodology by utilizing data from GISTDA, accessible through its disaster management portal. This platform provides critical geospatial information on flood events in Thailand, including downloadable shapefiles for spatial analysis across user-defined areas and timeframes. Accessing this data enables detailed and precise flood situation analysis. Additionally, the validation process integrates data from the Global Surface Water Explorer, a valuable tool for analyzing and monitoring global surface water changes. This tool is particularly useful for studying climate change impacts, hydrology, and environmental monitoring. Field surveys are also incorporated to enhance accuracy by providing localized and detailed ground-truth data essential for validating flood maps. Drone imagery plays a pivotal role in this process by offering high-resolution spatial data, which is especially valuable for assessing flood impacts in specific areas. Simultaneously, crowd-sourced data contributes real-time observations from diverse perspectives, reflecting on-ground realities and enriching the analysis. This multi-dimensional strategy strengthens the robustness of the validation process by combining authoritative reference data with field observations and community insights. By integrating diverse geospatial data sources, this approach ensures a thorough and reliable validation process.

3. Results

The Flood Impact Assessment Dashboard is a GEE application that offers comprehensive analysis and visualization of flood impacts across multiple dimensions. This powerful tool has been developed to examine flood effects on urban areas, agricultural lands, and population exposure, providing users with detailed insights into flood extent and its various consequences. Through its interactive map interface, users can easily navigate and examine different aspects of flood events. The dashboard offers the flexibility to toggle between various data layers, allowing for detailed visualization of flood impacts on different landscape features and infrastructure components. For those interested in exploring this comprehensive flood impact assessment tool further, the application is accessible at Thailand Flood Intelligence System.

Our system's UI interface allows users to select specific time frames for analyzing flood data across different years by inputting start and end dates for both pre-flood and post-flood periods. This flexibility enables users to explore flood data for any year within the available dataset, provided that Sentinel-1 imagery is available for those dates. However, GEE has limitations in terms of dynamic year selection and simultaneous comparison of flood data across multiple years. Users must manually input the desired date ranges for each analysis. While GEE does not natively support multi-year comparisons through a dropdown menu or similar interface, users can run separate analyses for different years and compare results manually.

To input new data, users can reload the page in their browser. This process allows them to start fresh with a new set of dates and analyze flood data for different periods. Despite these limitations, our interface provides a robust framework for analyzing flood data across various time frames, leveraging the strengths of Sentinel-1 imagery and GEE's processing capabilities. This research effectively addresses the challenges of varying spatial resolutions, integrates multi-temporal data, and mitigates potential discrepancies between datasets, resulting in a more accurate and reliable flood analysis. Leveraging the capabilities of GEE for geospatial data processing, the researchers maintained the native 10x10 meter resolution of Sentinel-1 SAR data while automatically resampling other relevant datasets to ensure compatibility. This was achieved through the utilization of functions such as clip, mosaic, and reducers. To integrate multi-temporal data, the researchers employed filtering and mosaicking techniques, segregating pre-flood and post-flood imagery before combining them into single composite images for each period.

Additionally, temporal reduction methods were applied to derive key statistics, such as total flood extent calculations. The study implemented several strategies to manage potential discrepancies. These included cloud masking by selecting images with less than 30% cloud cover, reducing SAR speckle noise through focal mean filtering, applying standardized thresholding for consistent flood area delineation across different time periods, and masking out permanent water bodies to isolate actual flood-affected areas. The details are as follows:

3.1 Flood Extent Mapping

The flood extent mapping methodology employs an advanced change detection approach using preprocessed Sentinel-1 SAR imagery. The process begins by calculating temporal backscatter differences between post-flood and pre-flood images through ratio-based analysis, effectively highlighting changes in surface water conditions while minimizing terrain and radar calibration effects. A critical threshold value of 1.30 is applied to create a binary flood extent mask, carefully calibrated through extensive testing to optimize the distinction between flooded and non-flooded areas. The resulting binary mask undergoes several refinement steps to enhance accuracy. A crucial step involves integrating the JRC Global Surface Water dataset to distinguish between flood waters and permanent water bodies. Areas containing water for more than 10 months annually are classified as permanent water bodies and excluded from flood extent calculations. The refinement process also includes spatial connectivity analysis, removing isolated pixels with fewer than eight connected neighbors to ensure coherent flood region identification.

Further refinement incorporates topographic constraints using SRTM DEM data. Areas with slopes exceeding 5 percent are masked out, as significant flooding is unlikely in steep terrain, thereby reducing false positives in mountainous regions. The final quantification converts the binary flood mask into actual area measurements by multiplying each identified flood pixel by its ground surface area, with results converted from square meters to square kilometers. The visualization clearly shows the effectiveness of this methodology, with the flood inundation map (rightmost image) precisely highlighting the spatial distribution of floodwater in blue. The consistent grayscale presentation of the base imagery in all three images helps identify subtle changes between pre and post-flood conditions, while the blue overlay in the flood inundation map provides clear indication of the flood's extent.

Chiang Rai, located in northern Thailand, is surrounded by prominent mountain ranges, including the Daen Lao range to the north, Doi Mae Salong and Doi Chang to the west, and the Phi Pan Nam range to the east. The province's major rivers include the Mekong, Kok, and Lao Rivers. Most flat areas are situated between valleys, forming high plains such as the Chiang Rai plateau. The region's hydrology is influenced by seasonal monsoons, with cooler temperatures during the northeast monsoon (October–February) and heavy rainfall during the southwest monsoon (May–October), which increases the risk of flash floods in valley areas [60].

Figure 3 illustrates a detailed flood extent mapping process using Sentinel-1 SAR satellite imageries, showcasing three distinct stages of analysis. The leftmost image captures the pre-flood conditions, providing a clear view of the natural terrain and landscape features before the flooding event occurred. This image serves as a baseline for understanding the area's normal state. The middle image represents the post-flood conditions, highlighting changes in the terrain caused by inundation. Finally, the rightmost image depicts the flood inundation extent, where flooded areas are distinctly marked in blue against a grayscale background, offering a visual representation of the affected regions. These images specifically depict the flood situation in Chiang Rai Province, Thailand, during September 2024.

Nong Khai, situated in the northeastern region of Thailand, is located within the low-lying plains of the Mekong River basin. The hydrology of this region is primarily governed by the seasonal fluctuations of the Mekong River, which experiences significant overflow during the southwest monsoon season (May–October). Heavy rainfall during this period exacerbates rising water levels, resulting in substantial flooding. The absence of upstream water management infrastructure further intensifies flood risks [61], as unregulated tributary flows contribute to inundation. This hydrological dynamic is clearly illustrated in Figure 4(c), where extensive portions of Nong Khai's low-lying plains are shown to be submerged under floodwaters. The blue zones in the map highlight areas most affected by flooding, particularly those near the riverbanks.

Phra Nakhon Si Ayutthaya, located in Thailand's lower Central Plains, is a flood-prone area characterized by flat terrain and extensive rice fields. Four major rivers the Chao Phraya, Pa Sak, Lopburi, and Noi flow through the province, interconnected by numerous canals. The rainy season (May–October), driven by the southwest monsoon, brings heavy rainfall, peaking in September. Figure 5(c) highlights flood dynamics during peak inundation, showing significant water coverage across agricultural lands and low-lying areas near riverbanks.

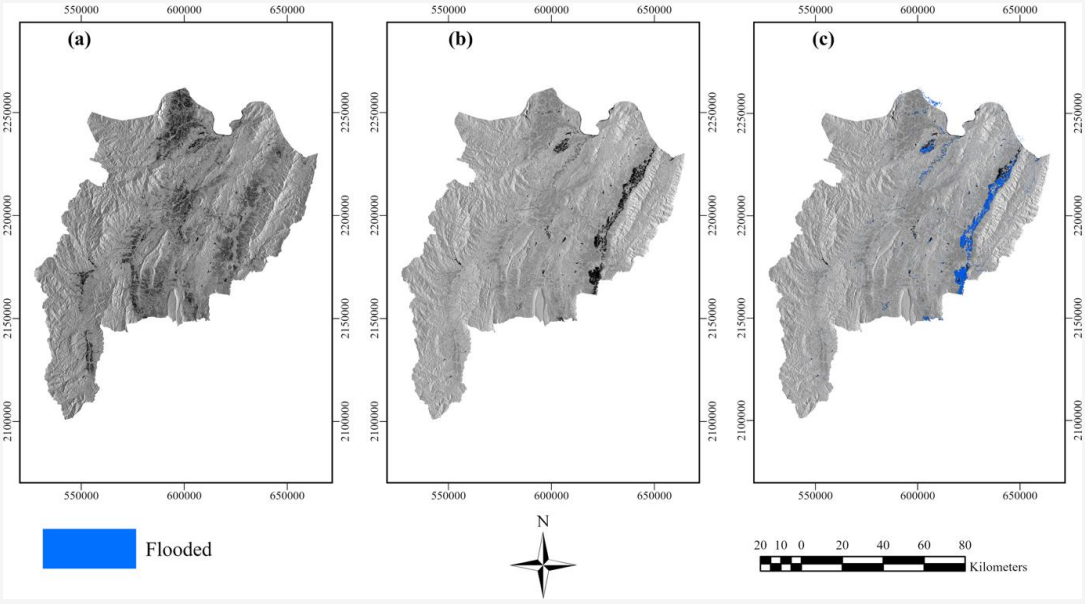

Figure 3: Visualization of Sentinel-1 SAR imagery in Chiang Rai:
(a) pre-flood (b) post-flood (c) flood inundation

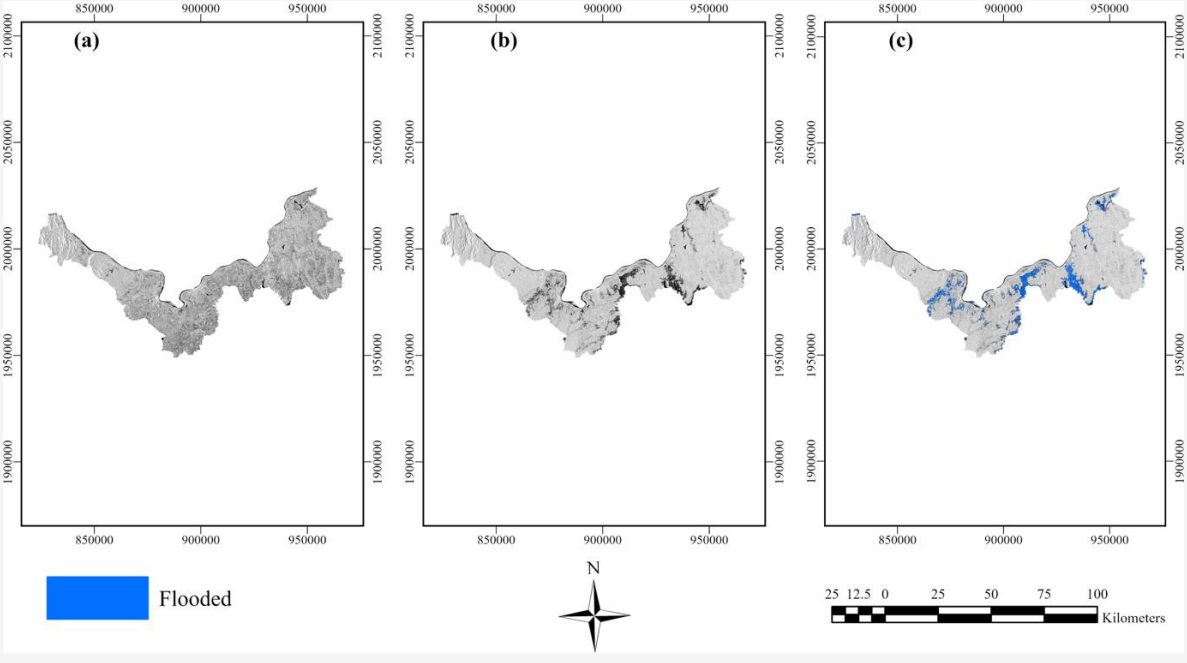

Figure 4: Visualization of Sentinel-1 SAR imagery in Nong Khai:
(a) pre-flood (b) post-flood (c) flood inundation

Kanchanaburi, in western Thailand, features forests, mountain ranges, valleys, and river plains. The rainy season (May–October), driven by the southwest monsoon, peaks in September with high humidity and heavy rainfall, supported by the province's extensive forest cover. Two major rivers, the Kwai Noi and Kwai Yai, shape the region's hydrology and increase flood risks. Figure 6(c) highlights flooded areas (blue zones), showing water coverage across valleys and low-lying areas near riverbanks.

Pattani, located in southern Thailand, is characterized by predominantly low-lying terrain suitable for agriculture, with sandy loam soil. The province has few mountains and is traversed by several rivers, including the Pattani, Saiburi, Yaring, and Nong Chik Rivers.

The rainy season lasts from mid-May to mid-October, driven by the southwest monsoon that covers Thailand. Additionally, low-pressure troughs occasionally affect southern Thailand during the early and late rainy season, contributing to widespread rainfall. Being situated on the eastern side of southern Thailand, Pattani also experiences rainfall during November and December due to the northeast monsoon passing over the Gulf of Thailand. Figure 7(c) illustrates Flood extent mapping distinctly marks flooded areas in blue against a grayscale background, emphasizing regions most affected by flooding. The visualization highlights agricultural lands and low-lying areas near rivers as the primary zones impacted by seasonal floods in Pattani Province.

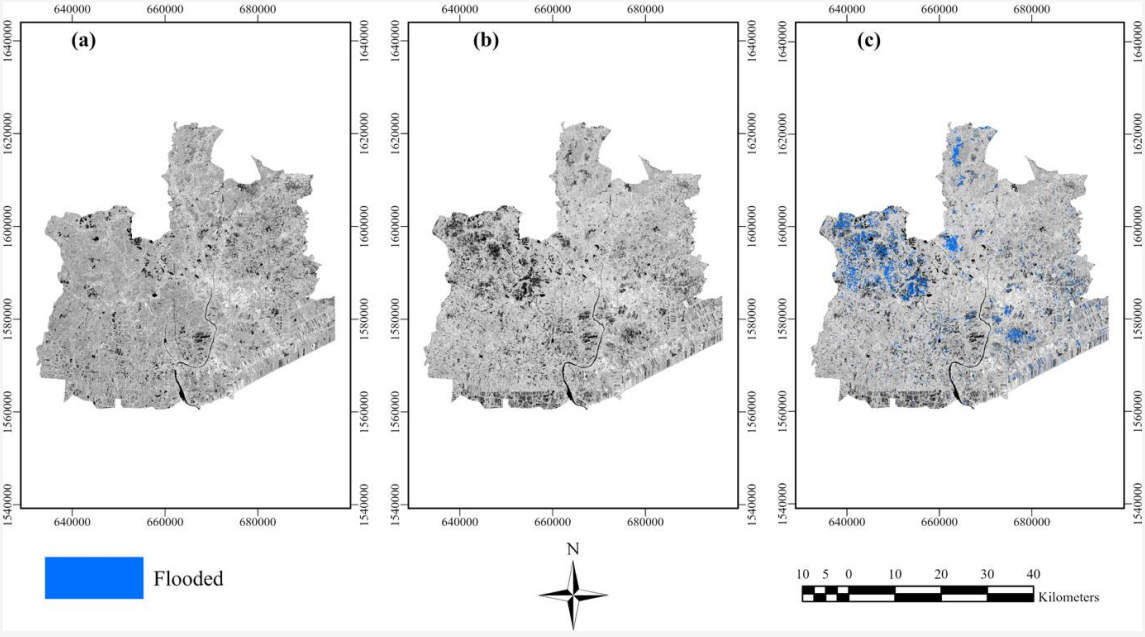

Figure 5: Visualization of Sentinel-1 SAR imagery in Phra Nakhon Si Ayutthaya:
(a) pre-flood (b) post-flood (c) flood inundation

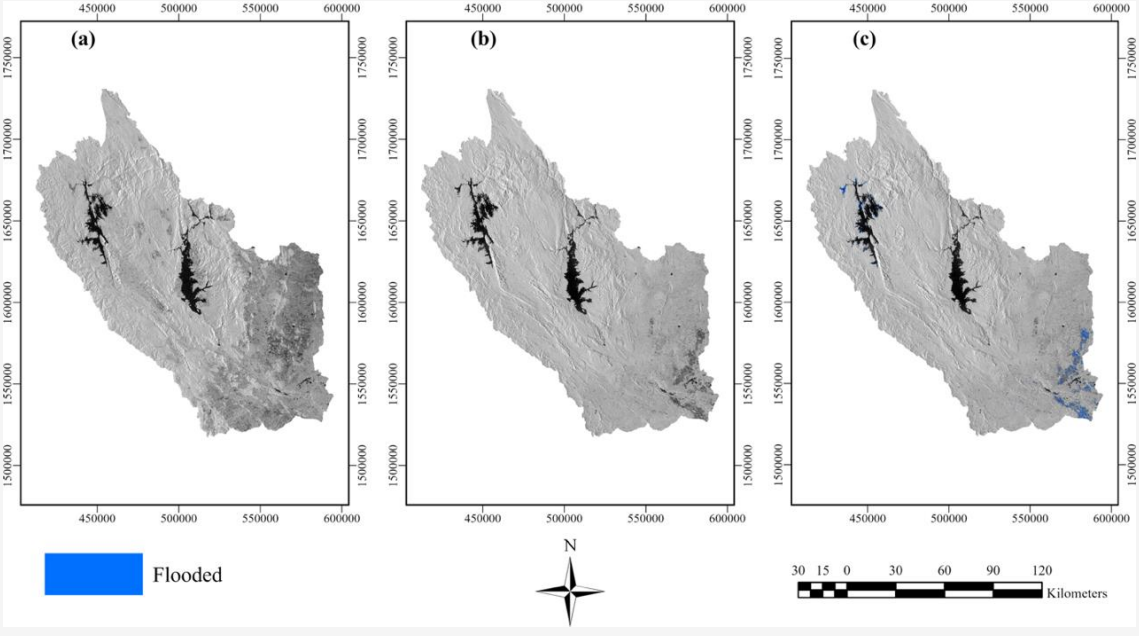

Figure 6: Visualization of Sentinel-1 SAR imagery in Kanchanaburi:
(a) pre-flood (b) post-flood (c) flood inundation

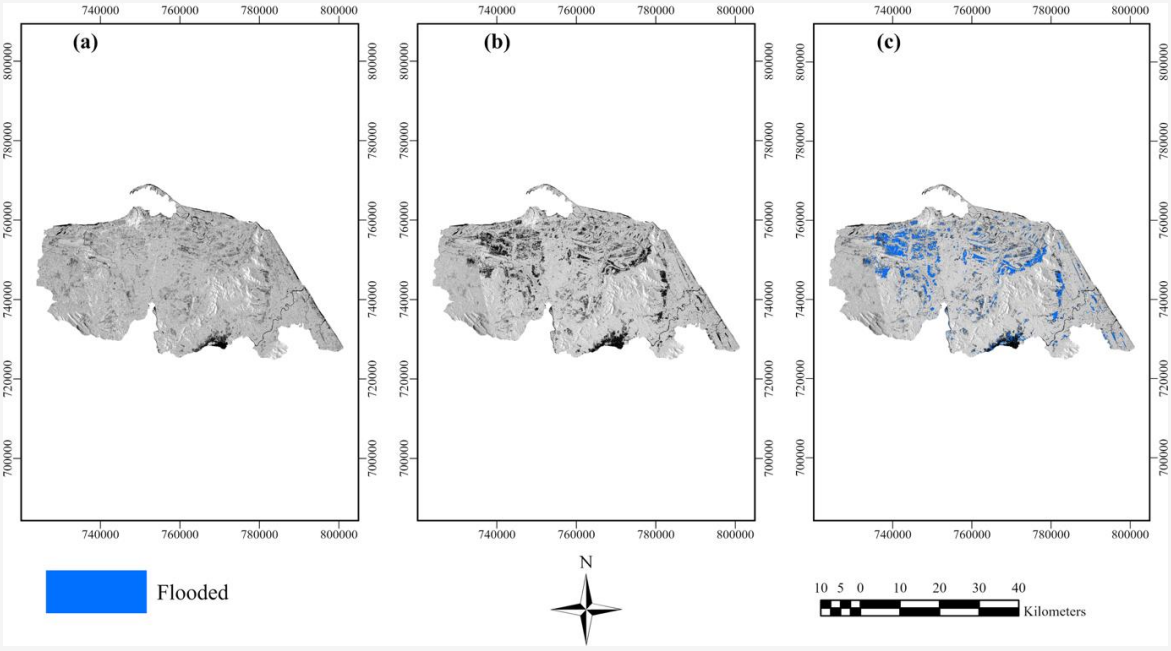

Figure 7: Visualization of Sentinel-1 SAR imagery in Pattani (a) pre-flood (b) post-flood (c) flood inundation

3.2 Geospatial Analysis for Flood Impact Assessment

The comprehensive visualization framework presented in Figures 8 demonstrates cutting-edge geospatial analysis techniques employed for flood impact assessment. These images showcase an intricate layering of data that enables thorough flood monitoring and analysis through various complementary perspectives. At the foundation of this analysis, Figure 8(a) showcases the ESA WorldCover's agricultural land classification, where cropland areas are prominently highlighted in yellow against detailed satellite imagery.

The visualization reveals a complex pattern of agricultural land distribution, particularly concentrated along the main transportation artery that bisects the image. The agricultural parcels vary in size and shape, with larger consolidated areas in the lower portion of the image and smaller, fragmented plots scattered throughout the urban fabric. This spatial arrangement demonstrates the interplay between agricultural activities and urban development, where farming practices persist within and around built-up areas. The high-resolution imagery allows for precise delineation of field boundaries, while the yellow overlay effectively distinguishes agricultural land from surrounding urban infrastructure and natural vegetation. This detailed mapping is crucial for understanding the agricultural landscape's vulnerability to flooding, as it clearly shows the proximity of croplands to urban areas and transportation networks. The pattern suggests a transitional zone where traditional agricultural practices meet urban expansion, highlighting the importance of preserving agricultural spaces within developing areas for food security and economic sustainability.

Building upon this agricultural foundation, Figure 8(b) showcases the ESA WorldCover built-up surface layer, where urban and developed areas are distinctly highlighted in magenta. This visualization powerfully demonstrates the spatial distribution of human settlements across the landscape, offering crucial insights into urbanization patterns and potential flood vulnerability. The stark magenta coloring creates a compelling visual contrast that clearly delineates the boundary between developed and undeveloped areas. This sharp distinction reveals intricate patterns of urban development, including dense settlement clusters, linear infrastructure corridors, and the gradual transition from urban cores to peripheral areas. The detailed 10-meter resolution of the WorldCover data allows for precise identification of individual buildings and urban structures, providing a comprehensive view of the built environment. From a flood vulnerability perspective, this visualization is particularly valuable as it highlights areas where human populations and infrastructure are concentrated. The clear demarcation of built-up surfaces helps identify zones where flood impacts could have the most significant socioeconomic consequences.

The spatial relationship between these developed areas and natural features like vegetation and water bodies, visible in the underlying imagery, offers critical context for assessing flood risk and planning mitigation strategies. The analysis gains additional depth through Figure 8(c), which presents GHSL Global population surfaces using an innovative gradient visualization. The carefully chosen purple and orange color scheme effectively communicates population density patterns, with vibrant orange areas signaling high-density populations and deeper purple indicating sparse settlement.

This sophisticated representation proves invaluable for identifying communities most vulnerable to flood impacts. Completing this multi-layered analysis, Figure 8(d) presents a sophisticated visualization of Google Research's Open Buildings dataset, where individual building footprints are meticulously delineated in red against high-resolution satellite imagery. The image reveals a complex urban fabric characterized by dense residential development along a major transportation corridor. The precise mapping of building outlines demonstrates varying structural densities, with larger commercial or institutional buildings interspersed among smaller residential structures. The detailed structural delineation showcases a well-organized urban layout, where buildings follow a clear grid pattern aligned with the main road network. This systematic arrangement reflects careful urban planning and development practices. The contrast between the red building footprints and the surrounding vegetation, visible in blue-green hues, highlights the interface between built and natural environments, providing valuable context for understanding urban expansion patterns.

This high-precision mapping serves multiple analytical purposes beyond basic building identification. The clear visualization of building sizes, shapes, and spatial relationships enables detailed analysis of urban morphology, population distribution patterns, and infrastructure requirements. Such granular data is particularly valuable for emergency response planning, as it provides exact building locations and access routes, critical for disaster management and evacuation planning.

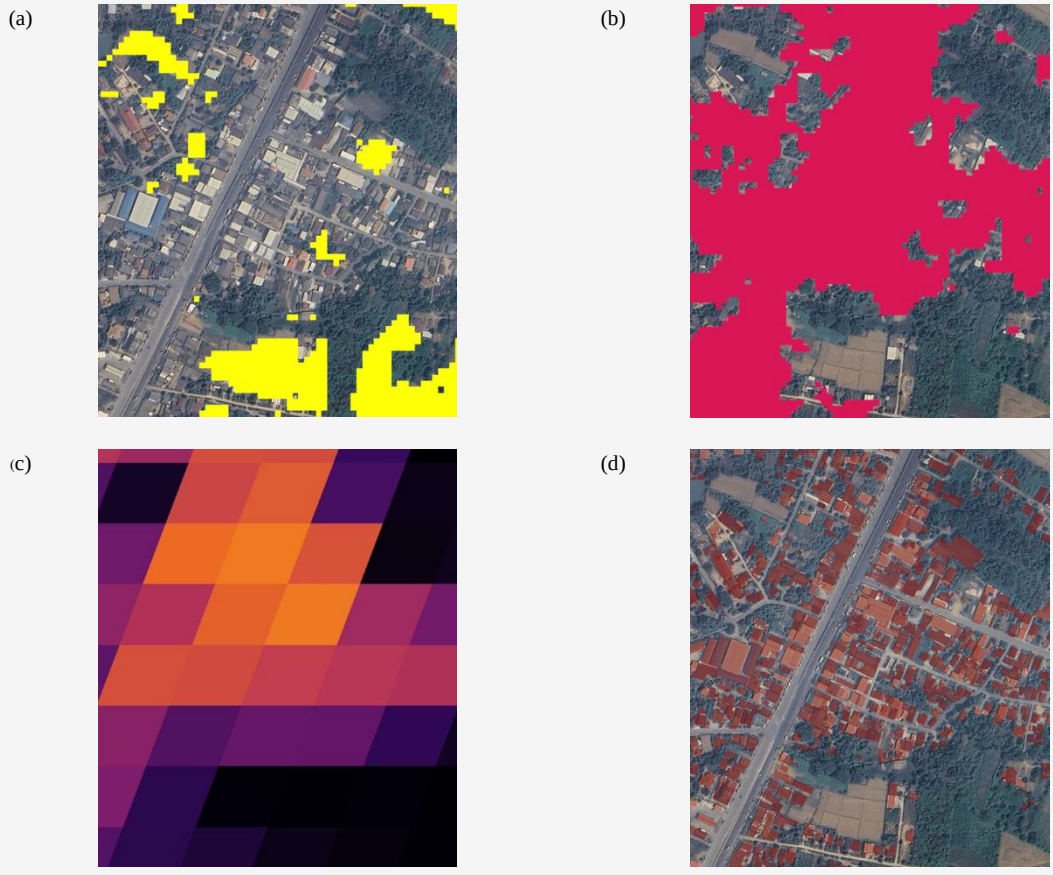

Figure 8: Geospatial data (a) agriculture area (b) urban area (c) global population surfaces (d) open buildings

Furthermore, the density and distribution patterns revealed in the imagery offer insights into local development trends, helping planners understand urban growth dynamics and make informed decisions about future infrastructure needs. The clear demarcation of individual structures also facilitates accurate assessment of potential flood impacts on the built environment, making it an invaluable tool for climate resilience planning.

The sequential integration of these diverse datasets creates a powerful analytical framework for understanding the complex interplay between human settlement patterns, agricultural activities, and flood vulnerability. This comprehensive approach enables emergency managers and urban planners to develop targeted flood mitigation strategies and response plans with unprecedented precision and effectiveness. Through this sophisticated visualization strategy, the analysis reveals the intricate relationships between different aspects of human settlement and economic activity, supporting more informed disaster preparedness and response planning. The combination of agricultural land use, built-up areas, population distribution, and building infrastructure data provides a holistic view of potential flood impacts, enabling more effective disaster management strategies.

3.3 A Comprehensive Analysis of Provincial Flood Monitoring and Impact Assessment

This Section delves into a comprehensive analysis of provincial flood monitoring and impact assessment, leveraging advanced geospatial tools and visualization techniques. This section highlights the integration of spatial and temporal parameters within a user-friendly interface designed to facilitate precise flood analysis at the provincial level. Figures 9 illustrate key components of this system, showcasing its capabilities in area selection, topographic analysis, and detailed impact assessment.

3.3.1 Figure 9(a): Provincial selection and time period interface for flood analysis

The interface displays Thailand's administrative boundaries with a focus on provincial-level selection capabilities. The map shows the country's provinces outlined in orange against a detailed topographic background, demonstrating the system's ability to facilitate precise area selection for flood analysis. The interface includes a time period selection panel that allows users to specify pre-flood and post-flood dates, enabling temporal analysis of flooding events. The visualization effectively combines geographical selection tools with temporal parameters, creating a user-friendly interface for comprehensive flood monitoring.

3.3.2 Figure 9(b): Detailed provincial view with topographic context

This visualization presents a closer examination of a selected province, highlighting the detailed topographic features that influence flood patterns. The terrain is rendered with high-resolution elevation data, showing the intricate relationship between landscape characteristics and potential flood vulnerability. The provincial boundaries are clearly delineated, and the surrounding topographic features, including mountains and valleys, are depicted in rich detail. This representation enables analysts to understand how terrain characteristics may affect flood behavior and impact assessment.

3.3.3 Figure 9(c): Flood impact assessment dashboard and visualization

The dashboard integrates flood impact metrics and spatial visualization in a sophisticated manner. On the left panel, key statistics are displayed, including the flood extent (19,788 km²), population exposure (6,392 people), and the number of flood-affected buildings (16,795 structures). The agricultural impact section indicates that out of a total agricultural area of 284,765 km², approximately 15,420 km² (5.41%) were affected by flooding. The urban flood impact analysis reveals that 1.23% of the total urban area (21,478 km²) experienced flooding, covering 264 km². The main map window presents these impacts through a multi-layer visualization, with flood-affected areas highlighted against the terrain background. The interface includes toggleable layers for various impact categories, allowing for detailed analysis of specific aspects of the flood event. This comprehensive visualization system effectively combines quantitative impact assessment with spatial analysis capabilities, providing decision-makers with crucial information for flood response and management strategies.

Table 3 and Table 4 summarize the flood extent and impacts across various provinces in Thailand during significant flood events in late 2024.

3.4 Validation of Sentinel-1 Satellite Imagery for Flood Mapping Accuracy in Thailand's Diverse Landscapes

The accuracy assessment of Sentinel-1 satellite imagery for flood mapping utilized a robust validation methodology across five geographically distinct provinces in Thailand. Figure 10 depicts flood extent and land use distribution for representative provinces from each region. In Figure 10(a), Chiang Rai is characterized by extensive agricultural areas and forested zones, which are prone to flooding due to its mountainous terrain and heavy rainfall.

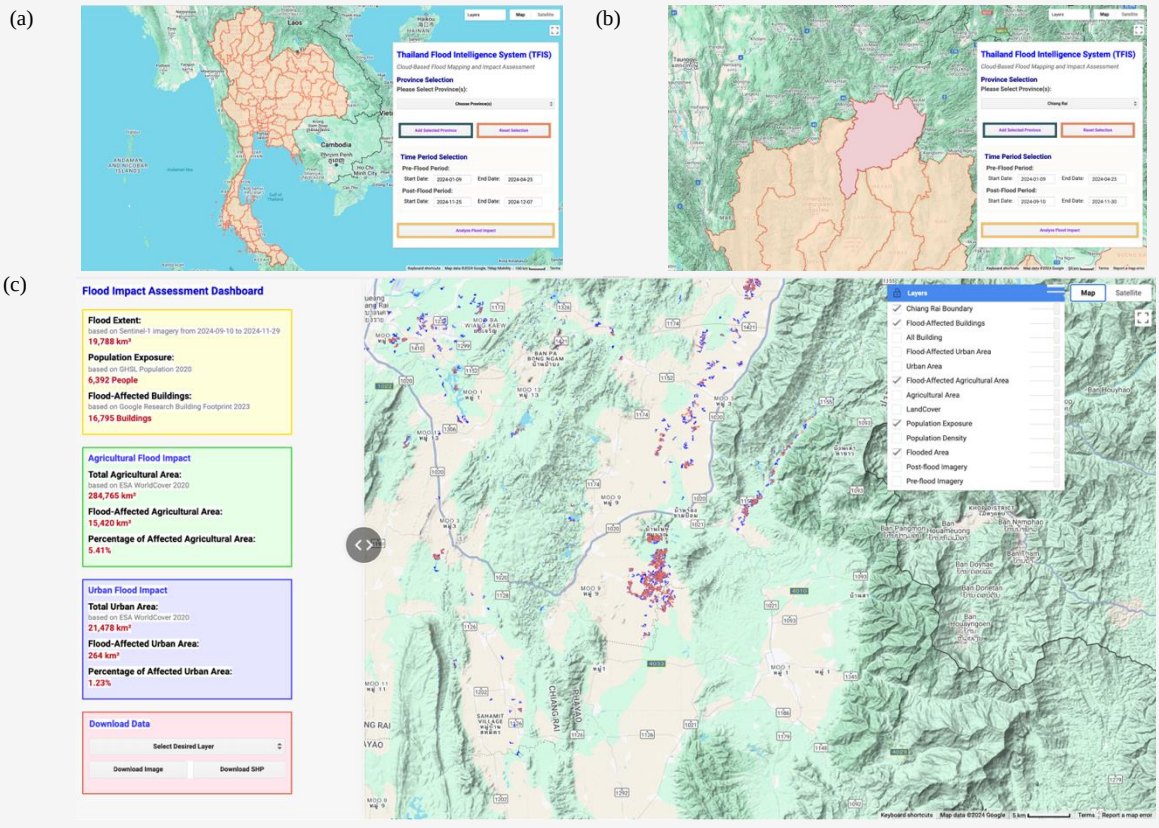

Figure 9: GEE-based flood monitoring system: (a) provincial selection and time period interface (b) topographic context (c) impact assessment dashboard

Table 3: Flood extent and impact by province

Province	Flood Extent (km²)	Population Exposure (People)	Flood-Affected Buildings (Buildings)
Chiang Rai: 6 September 2024	19,788	6,392	16,795
Phra Nakhon Si Ayudhya: 18 September 2024	9,002	3,800	33,520
Nong Khai: 8 September 2024	26,721	3,674	7,545
Kanchanaburi: 12 September 2024	12,863	564	4,882
Pattani: 4 December 2024	11,473	707	728

Table 4: Agricultural and urban flood impact by province

Province	Agricultural Flood Impact			Urban Flood Impact		
	Area (km²)	Flood-Affected Area (km²)	Affected Area (%)	Area (km²)	Flood-Affected Area (km²)	Affected area (%)
Chiang Rai	284,765	15,420	5.41	21,478	264	1.23
Phra Nakhon Si Ayudhya	163,834	7,009	0.79	20,937	523	0.05
Nong Khai	235,738	19,514	1.95	13,656	138	0.01
Kanchanaburi	379,183	9,815	0.98	14,975	66	0.01
Pattani	17,345	5,673	0.57	4,640	24	0.00

Figure 10(b) shows Nong Khai, featuring mixed land use with significant agricultural activity along the Mekong River, which frequently overflows during monsoons. Figure 10(c) illustrates Kanchanaburi, combining forested areas and agricultural lands dominated by sugarcane cultivation; its proximity to large dams increases susceptibility to controlled water releases during heavy rainfall.

Figure 10(d) highlights Phra Nakhon Si Ayutthaya, predominantly consisting of paddy fields and urban areas that serve as natural flood drainage zones during the wet season. Finally, Figure 10(e) represents Pattani, influenced by coastal geography with urban areas interspersed with agriculture and water bodies, making it vulnerable to both riverine and flash floods.

The error matrix presented in Table 5 provides detailed classification results for each province. The validation methodology employed a systematic random sampling approach with 512 points per each province to ensure comprehensive coverage and statistical robustness. This enhanced sampling strategy, utilizing 256 points each for flooded and non-flooded areas, effectively addressed the spatial heterogeneity inherent in flood mapping applications. The error matrix analysis revealed exceptional classification performance across diverse geographical contexts, with consistently high true positive rates for flood detection. The sampling design proved particularly effective in capturing the complex spatial patterns of flooding across Thailand's varied landscapes. The balanced distribution between flooded and non-flooded areas ensured unbiased representation despite the inherent imbalance in their spatial distribution. This methodology facilitated a robust statistical validation of classification results by comparing them with authoritative ground reference data from GISTDA, drone imagery, field surveys, and inquiries from local communities. The expanded sample size significantly enhanced the statistical significance of the accuracy assessment, providing comprehensive representation of classification performance across different landscape types. The systematic validation demonstrated strong agreement between satellite-derived classifications and ground reference data, with the error matrix documenting consistently high accuracy metrics across all study areas.

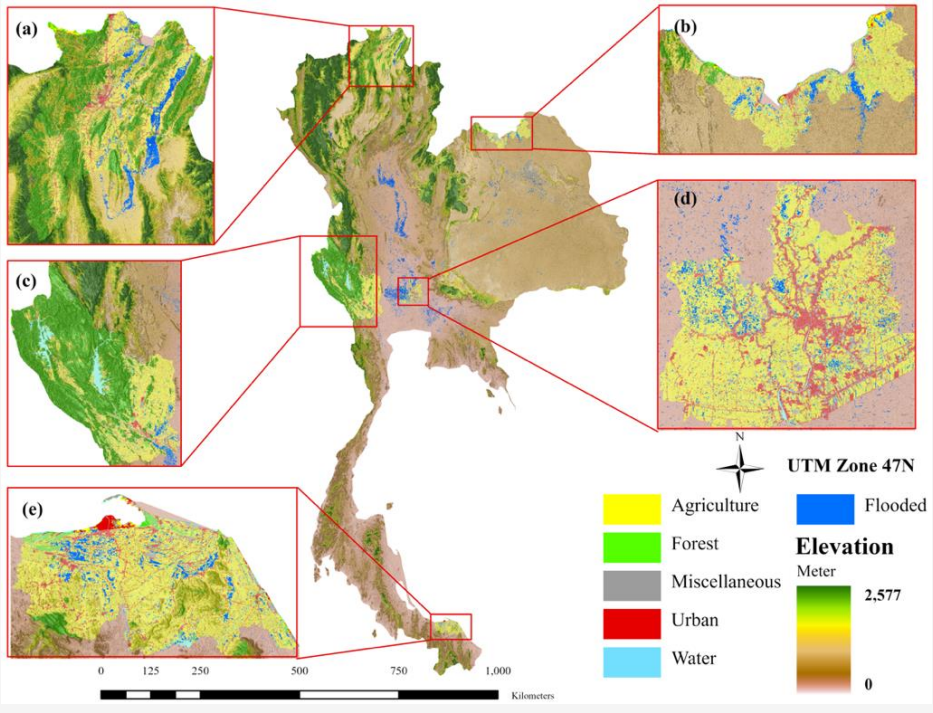

Figure 10: Flood extent in representative provinces from each region of Thailand that overlap with land use in: (a) Chiang Rai, (b) Nong Khai, (c) Kanchanaburi, (d) Phra Nakhon Si Ayutthaya, (e) Pattani

Table 5: Error matrix for provincial flood classifications using Sentinel-1 satellite imagery

Province	Date (2024)	Correct		Incorrect		OA	Kappa Coef.
		Flooded	Non-Flooded	Flooded	Non-Flooded		
Chiang Rai	6 Sep.	237	254	2	19	95.90	0.92
Nong Khai	8 Sep .	188	254	2	68	86.33	0.73
Kanchanaburi	12 Sep.	237	247	9	19	94.53	0.89
Phra Nakhon Si Ayutthaya	18 Sep .	247	248	8	9	96.67	0.93
Pattani	4 Dec.	252	256	0	4	99.21	0.98
					Average	**94.53**	**0.89**

The validation results demonstrated exceptional performance across all study regions, with particularly noteworthy outcomes in coastal and plains areas. Pattani province achieved the highest accuracy metrics with an overall accuracy of 99.21% and a kappa coefficient of 0.98, attributable to the distinct water-land interface characteristics of its coastal environment. Phra Nakhon Si Ayudhya province exhibited similarly impressive results with 96.67% overall accuracy and a kappa coefficient of 0.93, benefiting from its relatively uniform topography in the central plains. Chiang Rai province maintained high accuracy levels despite its challenging mountainous terrain, achieving 95.90% overall accuracy and a kappa coefficient of 0.92. Kanchanaburi province, characterized by forested areas and agricultural lands near large dams, achieved an overall accuracy of 94.53% and a kappa coefficient of 0.89, reflecting reliable classification performance. The most challenging environment was encountered in Nong Khai province, where the complex mixture of terrain types and varied land use patterns along the Mekong river resulted in an overall accuracy of 86.33% and a kappa coefficient of 0.73.

The methodology's effectiveness is evidenced by the system's overall performance metrics, which significantly exceeded established industry standards. The average overall accuracy of 94.53% substantially surpassed the 80% benchmark established by Congalton and Green [60], while the average kappa coefficient of 0.89 fell within the "Almost Perfect" category (0.81-1.00) according to Landis and Koch's assessment framework [62].

4. Discussion

This research demonstrates technical advancements through the development of an automated script suite designed to optimize flood mapping workflows on the GEE cloud platform using Sentinel-1 SAR data, marking a significant stride in rapid flood detection and impact assessment. However, the study revealed critical methodological limitations, particularly the temporal misalignment between satellite image acquisition and actual flood events. The Phayao Province case study starkly illustrates this issue: available satellite imagery from August 18 and 25, 2024, failed to capture the peak flooding on August 22, 2024. This temporal gap underscores a fundamental constraint in current satellite-based flood monitoring systems, especially for rapid-onset monsoon floods typical of Thailand’s climate.

The spatial resolution constraints of Sentinel-1 proved both advantageous and limiting. While sufficient for large-scale flood mapping, this resolution presents challenges in accurately delineating flood boundaries in complex urban environments and small agricultural parcels [63]. The study's accuracy assessment, though exceeding the conventional 80% threshold, suggests potential improvements through integration of higher-resolution data sources, particularly in areas with intricate land use patterns. Technical limitations extend beyond spatial resolution to include the inherent characteristics of SAR imagery processing. The speckle reduction techniques employed, while effective, may result in some loss of fine detail, particularly in areas with complex terrain or mixed land use. The implementation of the 50-meter circular kernel for noise reduction represents a compromise between detail preservation and processing efficiency that merits further optimization. The study's reliance on single-source satellite data, while demonstrating the capabilities of Sentinel-1, also reveals the potential benefits of multi-sensor integration.

Future methodological improvements could incorporate complementary data sources to create a more robust and comprehensive flood monitoring system. The integrating data from other sensors, such as optical imagery and weather models, can further enhance the system's capabilities. Optical imagery [64], like Sentinel-2, provides resolution visual data that can complement SAR's all-weather imaging, offering detailed insights into flood extent and impact, especially in clear weather conditions. Weather models can provide predictive insights into potential flood events, allowing for proactive measures. For instance, integrating precipitation forecasts from weather models with SAR data can improve flood prediction accuracy by anticipating areas at risk before the event occurs.

Machine learning techniques can also be integrated to enhance classification accuracy and automation. Studies have shown that combining dual-polarization SAR data (VV and VH) with machine learning models can improve flood detection [65], especially in complex environments. Furthermore, incorporating real-time ground observations and IoT devices can provide additional validation and complementary information for flood extent mapping, enhancing the system's reliability and responsiveness.

This research demonstrates the potential for scaling up the flood monitoring system by utilizing Sentinel-1 SAR imagery in conjunction with GEE, which enables the automated and accurate processing of large datasets. Additionally, integrating data from multiple sources, such as ESA WorldCover for land use analysis, GHSL for population assessment, and Microsoft Building Footprints for infrastructure mapping, allows for a comprehensive evaluation of flood impacts across multiple dimensions.

The application of this system in other regions can support disaster management efforts and reduce natural hazard risks, particularly flooding, which is a significant challenge faced by many countries worldwide. The use of standardized data and processing workflows makes this approach highly effective and adaptable for use in various regions.

The proposed approach to flood mapping using Sentinel-1 SAR data and GEE offers significant advancements in disaster response and management. However, it is crucial to acknowledge the potential limitations and sources of error in this process. One of the primary challenges in this approach is the impact of environmental factors on SAR data interpretation. Vegetation cover, for instance, can significantly affect the accuracy of flood mapping. Dense vegetation can obscure the radar signal, leading to underestimation of flood extent. Similarly, terrain slope can influence radar backscatter, potentially causing misclassification of flooded areas. The radar incidence angle also plays a role, as it can affect the signal's interaction with the ground surface, leading to variations in detected flood areas. Another limitation is the spatial resolution of the satellite imagery. Sentinel-1 SAR data, while highly effective for large-scale flood mapping, may not capture detailed features in areas with complex terrain, dense urban environments, or small agricultural parcels. This limitation can be mitigated by integrating Sentinel-1 SAR data with higher-resolution imagery from other sources, such as Planet Labs or WorldView, to enhance the accuracy of flood mapping in these challenging environments.

While GEE is a powerful platform for processing large-scale and diverse geospatial datasets, it faces limitations in real-time processing capabilities due to computational resource constraints, which can lead to latency in handling massive data volumes. Additionally, users may encounter challenges in customizing complex algorithms within GEE's predefined workflow frameworks. To address these constraints, potential solutions include optimizing GEE's computational infrastructure, implementing distributed data processing techniques to enhance efficiency, and integrating higher-resolution satellite imagery to improve analytical accuracy. For advanced algorithmic customization or resource-intensive tasks, complementing GEE with external tools such as ArcGIS or Python-based frameworks (e.g., GDAL, TensorFlow) may offer greater flexibility and precision.

Combining satellite imagery with different spatial resolutions in GEE can be achieved through resampling and reprojection techniques to ensure that all images have the same resolution and coordinate system. Initially, the resample method should be used to adjust the resolution of the images to match, with options for 'bilinear' resampling for continuous data or 'nearest neighbor' for categorical data. Following this, reproject is used to align the coordinate systems. For data with lower resolutions, reduce Resolution can be employed to reduce the resolution by statistically aggregating pixel values, such as using ee.Reducer.mean() to preserve the statistical properties of the original data. Finally, after aligning the resolutions and projections, the merge function can be used to combine the datasets, but it is crucial to ensure that the band names and properties of all images are consistent for successful merging.

The research also underscores the importance of considering seasonal variations and long-term temporal coverage in flood monitoring methodologies. The current approach, while effective for individual flood events, could benefit from incorporating seasonal baseline data and historical flood patterns to improve detection accuracy and provide context for impact assessments. These methodological insights suggest several key directions for future research. The development of advanced algorithms for temporal interpolation could help address the challenges of image acquisition timing. Integration of multiple satellite platforms could improve both spatial and temporal resolution. The limitations identified in this study serve not as impediments but as valuable guideposts for future methodological improvements. The demonstrated success of cloud-based processing, combined with the identified areas for enhancement, provides a solid foundation for developing more sophisticated and reliable flood monitoring systems. These advancements will be crucial for supporting effective disaster response and management strategies in Thailand's diverse and challenging geographical context.

5. Conclusion

This research marks a pivotal breakthrough in flood monitoring technology by integrating Sentinel-1 SAR imagery with the cloud computing capabilities of GEE through a cloud-based platform. The methodology aligns with the UN-SPIDER recommended practices for flood mapping, employing a change detection approach to identify flooded areas by comparing pre-flood and post-flood images. This technique effectively highlights changes in surface water conditions while minimizing terrain and radar calibration effects.

A critical threshold value of 1.30 is applied to binarize the ratio of post-flood to pre-flood backscatter values, optimizing the balance between detecting true flood areas and minimizing false positives.

The use of VH polarization is preferred due to its sensitivity to surface changes and lower susceptibility to double-bounce effects compared to VV polarization, making it particularly suitable for flood mapping. The integration of JRC Global Surface Water data helps distinguish between floodwaters and permanent water bodies, ensuring accurate delineation of inundated areas. Additionally, spatial connectivity analysis and topographic constraints using SRTM elevation data further refine the flood extent mapping by eliminating isolated pixels and areas with slopes exceeding 5 percent, enhancing the system's reliability in complex terrain environments.

Speckle filtering is a crucial step in enhancing flood map accuracy, employing area-based techniques to reduce noise in SAR images while preserving critical flood extent information. The 50-meter circular kernel effectively reduces noise without excessive blurring, preserving flood boundary details in complex terrain. The integration of multi-source data—ESA WorldCover (land use), GHSL (population), and Microsoft Building Footprints (infrastructure)—enables comprehensive flood impact analysis, particularly for agriculture, population, and infrastructure. These data are vital for efficient disaster response planning and resource allocation. The comprehensive assessment framework developed in this study offers unprecedented multi-dimensional insights into flood-affected areas.

The analysis of five provinces Chiang Rai, Nong Khai, Kanchanaburi, Phra Nakhon Si Ayudhya and Pattani reveals consistent patterns of agricultural vulnerability, with significant implications for economic stability and food security. The system's ability to quantify impacts on population, infrastructure, and agricultural areas provides crucial decision support for emergency response and resource allocation. The validation results demonstrate exceptional performance across diverse geographical contexts, with an average accuracy of 94.53% and a mean kappa coefficient of 0.89, significantly exceeding conventional industry standards. This robust validation process ensures the reliability of the resulting flood maps, providing critical insights for disaster response and resource allocation.

This research makes several significant contributions to the field of disaster management. First, it demonstrates the feasibility of cloud-based processing for rapid flood mapping at provincial scales. Second, it establishes a robust methodology for integrating multiple geospatial datasets to provide comprehensive impact assessments. Third, it offers a scalable framework that can be adapted to other regions facing similar flooding challenges. The findings underscore the critical need for technological in addressing Thailand's persistent flooding challenges. The developed system not only provides immediate practical value for disaster response but also establishes a foundation for long-term resilience building. The integration of cloud computing, earth observation, and advanced analytical techniques represents a significant step forward in Thailand's capacity to monitor, respond to, and mitigate flood impacts.

Looking forward, this research opens new avenues for enhancing disaster management capabilities through technology. The demonstrated success in combining multiple data sources and analytical techniques suggests potential applications beyond flood monitoring, extending to other natural hazards and environmental challenges. The system's architecture provides a blueprint for developing similar applications in other regions, contributing to global efforts in disaster risk reduction and climate change adaptation.

6. Future Research and Recommendations

The findings of this study provide a robust foundation for flood monitoring and impact assessment using Sentinel-1 SAR imagery and GEE. However, there are several avenues for future research and improvements that could enhance the accuracy and applicability of this approach. One key area for future research is the optimization of polarization selection for flood mapping. While VH polarization is generally preferred due to its sensitivity to surface changes, a comprehensive analysis of polarization ratios, particularly VH/VV, could provide valuable insights into vegetation phenology and water content assessment. This analysis could lead to more nuanced flood mapping techniques, especially in areas with complex vegetation cover.

The threshold value of 1.30 used in this study for change detection was determined through extensive experimentation. However, future research should focus on developing adaptive thresholding techniques that can account for local conditions, specific flood characteristics, and varying polarization modes. This could involve the integration of machine learning algorithms within the GEE platform to automatically determine optimal thresholds for different geographical and environmental contexts. To further enhance the accuracy of flood mapping, future studies should explore the integration of additional datasets. For instance, high-resolution digital elevation models could improve the delineation of flood extents in areas with complex topography.

Additionally, the incorporation of soil moisture data could provide valuable information on antecedent conditions that influence flood susceptibility.

Future research should focus on developing advanced speckle filtering techniques to enhance flood mapping accuracy. While the current approach uses a focal mean filter, adaptive methods such as Gamma-MAP, Frost, or Lee Sigma filters could better preserve fine details while reducing noise [66][67] and [68]. These filters are not standard in GEE but can be manually implemented using JavaScript for customization. GEE also provides built-in functions like focal_mean and focal_median, which are user-friendly but less effective for advanced noise reduction. The trade-off lies between the simplicity of built-in functions and the precision of custom filters, requiring a deeper understanding of both filtering methods and the GEE platform.

Furthermore, future studies should focus on validating and calibrating the flood mapping results against a wider range of reference data sources. This could include high-resolution optical imagery and ground-based observations. Such comprehensive validation efforts would not only improve the accuracy of the flood maps but also help in understanding the limitations and uncertainties associated with SAR-based flood mapping.

Lastly, future research should explore the potential of multi-temporal analysis techniques. By analyzing longer time series of Sentinel-1 data, it may be possible to develop more robust change detection methods that can better distinguish between temporary flood events and long-term changes in surface water dynamics.

References

[1] Drought and Flood Risk Situation in Thailand, (2024). MS&AD InterRisk Research & Consulting. [Online]. Available: https://www.interriskthai.co.th/blog/drought-and-flood-risk-situation-in-thailand-updated-august-2024/. [Accessed: Oct. 14, 2024].

[2] Lwin, P., (2024). Thailand's Innovative Approaches to Flood Management. TThaiger. [Online]. Available: https://thethaiger.com/thai-life/thailands-innovative-approaches-to-flood-management. [Accessed: Oct. 14, 2024].

[3] Daily Weather Forecast Report, (2024). Thai Meteorological Department. [Online]. Available: https://www.tmd.go.th/weather/weatherthailand. [Accessed: Oct. 14, 2024].

[4] Tarpanelli, A., Mondini, A. C. and Camici, S., (2022). Effectiveness of Sentinel-1 and Sentinel-2 for Flood Detection Assessment in Europe. *Natural Hazards and Earth System Sciences*, Vol. 22, 2473-2489. https://doi.org/10.5194/nhess-22-2473-2022.

[5] Sentinel-1 Instrument Overview. European Space Agency. [Online]. Available: https://earth.esa.int/eogateway/documents/20142/37627/2-Sentinel -1_Instrument_Overview. pdf. [Accessed: Oct. 14, 2024].

[6] Torres, R., Snoeij, P., Geudtner, D., Bibby, D., Davidson, M., Attema, E., Potin, P., Rommen, B., Floury, N., Brown, M., Traver, I. N., Deghaye, P., Duesmann, B., Rosich, B., Miranda, N., Bruno, C., L'Abbate, M., Croci, R., Pietropaolo, A., Huchler, M. and Rostan, F., (2012). GMES Sentinel-1 Mission. *Remote Sensing of Environment*, Vol. 120, 9-24. https://doi.org/10.1016/j.rse.2011.05.028.

[7] Potin, P., Rosich, B., Miranda, N., Grimont, P., Shurmer, I., O'Connell, A., Krassenburg, M. and Gratadour, J. B., (2019). Copernicus Sentinel-1 Constellation Mission Operations Status. *IEEE International Geoscience and Remote Sensing Symposium*, 5385-5388. https://doi.org/10.1109/IGARSS.2019.8898949.

[8] Data Products. European Space Agency. [Online]. Available: https://www.esa.int/Applications/Observing_the_Earth/Copernicus/Sentinel-1/Data_products. [Accessed Oct. 14, 2024].

[9] De Zan, F. and Guarnieri, A. M., (2006). TOPSAR: Terrain Observation by Progressive Scans. *IEEE Transactions on Geoscience and Remote Sensing*, Vol. 44(9), 2352-2360. https://doi.org/10.1109/TGRS.2006.873853.

[10] Sentinel-1: ESA's Radar Observatory Mission for GMES Operational Services. European Space Agency. [Online]. Available: https://sentinel.esa.int/documents/247904/349449/S1_SP-1322_1.pdf. [Accessed: Oct. 17, 2024].

[11] Sentinel 1 Satellite Images. EOS Data Analytics. [Online]. Available: https://eos.com/find-satellite/sentinel-1/. [Accessed: Oct. 17, 2024].

[12] Overview of Sentinel-1 Mission. European Space Agency. [Online]. Available: https://sentiwiki.copernicus.eu/web/s1-mission. [Accessed: Oct. 17, 2024].

[13] Gorelick, N., Hancher, M., Dixon, M., Ilyushchenko, S., Thau, D. and Moore, R., (2017). Google Earth Engine: Planetary-Scale Geospatial Analysis for Everyone. *Remote Sensing of Environment*, Vol. 202, 18-27. https://doi.org/10.1016/j.rse.2017.02.021.

[14] Kumar, L. and Mutanga, O., (2018). Google Earth Engine Applications Since Inception: Usage, Trends, and Potential. *Remote Sensing*, Vol. 10(10). https://doi.org/10.3390/rs10101509.

[15] Tamiminia, H., Salehi, B., Mahdianpari, M., Quackenbush, L., Adeli, S. and Brisco, B., (2020). Google Earth Engine for Geo-Big Data Applications: A Meta-Analysis and Systematic Review. *ISPRS Journal of Photogrammetry and Remote Sensing*, Vol. 164, 152-170. https://doi.org/10.1016/j.isprsjprs.2020.04.001.

[16] Amani, M., Ghorbanian, A., Ahmadi, S. A., Kakooei, M., Moghimi, A., Mirmazloumi, S. M. and Brisco, B., (2020). Google Earth Engine Cloud Computing Platform for Remote Sensing Big Data Applications: A Comprehensive Review. *IEEE Journal of Selected Topics in Applied Earth Observations and Remote Sensing*, Vol. 13, 5326-5350. https://doi.org/10.1109/JSTARS.2020.3021052.

[17] Recommended Practice: Flood Mapping and Damage Assessment Using Sentinel-1 SAR Data in Google Earth Engine. United Nations Platform for Space-based Information for Disaster Management and Emergency Response (UN-SPIDER). [Online]. Available: https://www.un-spider.org/advisory-support/recommended-practices/recommended-practice-google-earth-engine-flood-mapping/step-by-step [Accessed: Nov. 13, 2024].

[18] Singh, G. and Rawat, K. S., (2024). Mapping Flooded Areas Utilizing Google Earth Engine and Open SAR Data: A Comprehensive Approach for Disaster Response. *Discoveries in Geoscience*, Vol. 2(5). https://doi.org/10.1007/s44288-024-00006-4.

[19] Khamphilung, P., Konyai, S., Slack, D., Chaibandit, K. and Prasertsri, N., (2023). Flood Event Detection and Assessment using Sentinel-1 SAR-C Time Series and Machine Learning Classifiers Impacted on Agricultural Area, Northeastern, Thailand. *International Journal of Geoinformatics*, Vol. 19(6), 17–29. https://doi.org/10.52939/ijg.v19i6.2691.

[20] Thammaboribal, P., Tripathi, N., Lipiloet, S. and Mandadi, R., (2025). Flood Mapping and Damage Assessment Using UN-SPIDER Recommended Practices in Google Earth Engine: A Case Study of the 2024 Chiang Rai Flood, Thailand. *International Journal of Geoinformatics*, Vol. 21(3), 165–179. https://doi.org/10.52939/ijg.v21i3.4039.

[21] Hamidi, E., Peter, B. G., Muñoz, D. F., Moftakhari, H. and Moradkhani, H., (2023). Fast Flood Extent Monitoring with SAR Change Detection Using Google Earth Engine. *IEEE Transactions on Geoscience and Remote Sensing*, Vol. 61, 1-19. https://doi.org/10.1109/TGRS.2023.3240097.

[22] Nguyen, D., Chou, T., Hoang, T. and Chen, M., (2023). Flood Susceptibility Mapping Using Machine Learning Algorithms: A Case Study in Huong Khe District, Ha Tinh Province, Vietnam. *International Journal of Geoinformatics*, Vol. 19(7), 1–15. https://doi.org/10.52939/ijg.v19i7.2739.

[23] Boonma, R., Suwanprasit, C., Homhuan, S. and Shahnawaz, . (2024). Classification of Northern Thai Rice Varieties Using Random Forest (RF) and Support Vector Machine (SVM) on Google Earth Engine with Sentinel Imagery: A Case Study in Buak Khang Subdistrict, San Kamphaeng District, Chiang Mai Province. *International Journal of Geoinformatics*, Vol. 20(9), 27–42. https://doi.org/10.52939/ijg.v20i9.3539.

[24] Boonma, R., Suwanprasit, C. and Homhuan, S., (2024). Modeling Rice Growth and Yield using Integrated Remote Sensing Data on Google Earth Engine. *International Journal of Geoinformatics*, Vol. 20(11), 116–133. https://doi.org/10.52939/ijg.v20i11.3693.

[25] Luo, C., Liu, H., Lu, L., Liu, Z., Kong, F. and Zhang, X., (2021). Monthly Composites from Sentinel-1 and Sentinel-2 Images for Regional Major Crop Mapping with Google Earth Engine. *Journal of Integrative Agriculture*, Vol. 20(7), 1944-1957. https://doi.org/10.1016/S2095-3119(20)63329-9.

[26] Anucharn, T., Hongpradit, P., Iamchuen, N. and Puttinaovarat, S., (2025). Spatial Analysis of Urban Expansion and Energy Consumption Using Nighttime Light Data: A Comparative Study of Google Earth Engine and Traditional Methods for Improved Living Spaces. *ISPRS International Journal of Geo-Information*, Vol. 14(4). https://doi.org/10.3390/ijgi14040178.

[27] Sun, Z., Xu, R., Du, W., Wang, L. and Lu, D., (2019). High-Resolution Urban Land Mapping in China from Sentinel 1A/2 Imagery Based on Google Earth Engine. *Remote Sensing*, Vol. 11(7). https://doi.org/10.3390/rs11070752.

[28] Geographic Regionalization. Office of the Royal Society. [Online]. Available: http://legacy.orst.go.th/?knowledges=การแบ่งภูมิภาคทางภูมิศe. [Accessed: Oct. 24, 2024].

[29] Floods Directive GIS Guidance. Directorate-General for the Environment, European Commission. Available: https://cdr.eionet.europa.eu/help/Floods/Floods_2018/GuidanceDocuments/Floods_GISGuidance.pdf. [Accessed Oct. 24, 2024].

[30] Dhanabalan, S. P., Abdul Rahaman, S. and Jegankumar, R., (2021). Flood Monitoring Using Sentinel-1 Sar Data: A Case Study Based on an Event of 2018 and 2019 Southern Part of Kerala. *Int. Arch. Photogramm. Remote Sensing and Spatial Information Sciences,* Vol. XLIV-M-3-2021, 37-41. https://doi.org/10.5194/isprs-archives-XLIV-M-3-2021-37-2021.

[31] Sentinel-1 SAR GRD: C-band Synthetic Aperture Radar Ground Range Detected, log scaling. Earth Engine Data Catalog. [Online]. Available: https://developers.google.com/earth-engine/datasets/catalog/COPERNICUS_S1_GRD. [Accessed: Sep. 11, 2024].

[32] Sentinel 1 Level-1 Ground Range Detected (GRD). United Nations Development Programme. [Online]. Available: https://geohub.data.undp.org/data/e95f5f75df0b536378becbfa67a2a064. [Accessed: Sep. 11, 2024].

[33] About Sentinel-1 GRD Data. Sentinelhub. [Online]. Available: https://docs.sentinel-hub.com/api/latest/data/sentinel-1-grd/. [Accessed: Sep. 11, 2024].

[34] Sentinel-1 GRD. Copernicus Data Space Ecosystem. [Online]. Available: https://documentation.dataspace.copernicus.eu/APIs/SentinelHub/Data/S1GRD.html. [Accessed: Sep. 11, 2024].

[35] Sentinel-1 SAR GRD: C-band Synthetic Aperture Radar Ground Range Detected, Log Scaling. Earth Engine Data Catalog. [Online]. Available: https://developers.google.com/earth-engine/da tasets/catalog/COPERNICUS_S1_GRD#bands. [Accessed: Sep. 11, 2024].

[36] GloFAS Global Flood Monitoring (GFM). Copernicus Programme. [Online]. Available: https://global-flood.emergency.copernicus.eu/technical-information/glofas-gfm/. [Accessed: Sep. 11, 2024].

[37] Sentinel-1 Applications. European Space Agency. Available: https://sentiwiki.copernicus.eu/web/s1-applications. [Accessed Nov. 13, 2024].

[38] Baghdadi, N., Bernier, M., Gauthier, R. and Neeson, I., (2001). Evaluation of C-Band SAR Data for Wetlands Mapping. *International Journal of Remote Sensing,* Vol. 22(1), 71-88. https://doi.org/10.1080/014311601750038857.

[39] Guihong, L., Xiaofeng, Y., Xiaofeng, L., Biao, Z., William, P., Ziwei, L. and Xuan Z., (2013). A Systematic Comparison of the Effect of Polarization Ratio Models on Sea Surface Wind Retrieval from C-Band Synthetic Aperture Radar. *IEEE Journal of Selected Topics in Applied Earth Observations and Remote Sensing,* Vol. 6(3),1100-1108. https://doi.org/10.1109/JSTARS.2013.2242848.

[40] Amitrano, D., Guida, R. and Ruello, G., (2019). Multitemporal SAR RGB Processing for Sentinel-1 GRD Products: Methodology and Applications. *IEEE Journal of Selected Topics in Applied Earth Observations and Remote Sensing,* Vol. 12(5), 1497-1507. https://doi.org/10.1109/JSTARS.2019.2904035.

[41] Dang, B., (2024). *Comparison of Polarization Models in SAR Technology for Water Body Extraction.* KTH Royal Institute of Technology. [Online]. Available: https://kth.diva-portal.org/smash/get/diva2:1901548/FULLTEXT01.pdf. [Accessed: Nov. 13, 2025].

[42] Faizan, M. and Palanisamy, G., (2021). *Mapping of Flood Areas Using Sentinel-1 Synthetic Aperture Radar (SAR) Images with Google Earth Engine Cloud Platform - A Case Study of Chamoli District, Uttarakhand- India*. 3rd ed., Intercontinental Geoinformation Days (IGD). Turkey: Mersin, 2021, 18-21.

[43] FAO GAUL: Global Administrative Unit Layers 2015, First-Level Administrative Units. Earth Engine Data Catalog. [Online]. Available: https://developers.google.com/earth-engine/datasets/catalog/FAO_GAUL_2015_level1. [Accessed: Sep. 11, 2024].

[44] Pekel, J. F., Cottam, A., Gorelick, N. and Belward, A. S., (2016). High-Resolution Mapping of Global Surface Water and Its Long-Term Changes. *Nature*, Vol. 540, 418-422. https://doi.org/10.1038/nature20584.

[45] Zanaga, D., Van De Kerchove, R., De Keersmaecker, W., Souverijns, N., Brockmann, C., Quast, R., Wevers, J., Grosu, A., Paccini, A., Vergnaud, S., Cartus, O., Santoro, M., Fritz, S., Georgieva, I., Lesiv, M., Carter, S., Herold, M., Li, L., Tsendbazar, N. E., Ramoino, F. and Arino, O., (2024). ESA WorldCover 10 m 2020 v100. *Zenodo.* Available: https://zenodo.org/records/5571936. [Accessed Sep. 11, 2024].

[46] Farr, T. G., Rosen, P. A., Caro, E., Crippen, R., Duren, R., Hensley, S., Kobrick, M., Paller, M., Rodriguez, E., Roth, L., Seal, D., Shaffer, S., Shimada, J., Umland, J., Werner, M., Oskin, M., Burbank, D. and Alsdorf, D. E., (2007). The Shuttle Radar Topography Mission. *Reviews of*

Geophysics, Vol. 45(2). https://doi.org/10.1029/2005RG000183.

[47] Carioli, A., Schiavina, M., Freire, S. and MacManus, K., (2023). GHS Population Grid Multitemporal (1975-2030). *European Commission, Joint Research Centr*e. [Online]. Available: https://doi.org/10.2905/2FF68A52-5B5B-4A22-8F40-C41DA8332CFE. [Accessed: Sep. 11, 2024].

[48] Sirko, W., Kashubin, S., Ritter, M., Annkah, A., Bouchareb, Y.S.E., Dauphin, Y., Keysers, D., Neumann, M., Cisse, M. and Quinn, J. A., (2023). Open Buildings V3 Polygons. Earth Engine Data Catalog. [Online]. Available: https://developers.google.com/earth-engine/datasets/catalog/GOOGLE_Research_open-buildingsv3polygons. [Accessed: Sep. 11, 2024].

[49] Huang, L., Liu, B., Li, X., Zhang, Z. and Yu, W., (2017). Technical Evaluation of Sentinel-1 IW Mode Cross-pol Radar Backscattering from the Ocean Surface in Moderate Wind Condition. *Remote Sensing*, Vol. 9(8). https://doi.org/10.3390/rs9080854.

[50] Qiu, F., Berglund, J., Jensen, J., Thakkar, P. and Ren, D., (2004). Speckle Noise Reduction in SAR Imagery Using a Local Adaptive Median Filter. *GIScience & Remote Sensing*, Vol. 41(3), 244-266. https://doi.org/10.2747/1548-1603.41.3.244.

[51] Frost, V. S., Stiles, J. A., Shanmugan, K. S. and Holtzman, J. C., (1982). A Model for Radar Images and Its Application to Adaptive Digital Filtering of Multiplicative Noise. *IEEE Transactions on Pattern Analysis and Machine Intelligence*. Vol. PAMI-4(2), 157-166. https://doi.org/10.1109/TPAMI.1982.4767223.

[52] Lee, J. S., (1980). Digital Image Enhancement and Noise Filtering by Use of Local Statistics. *IEEE Transactions on Pattern Analysis and Machine Intelligence*. Vol. PAMI-2(2), 165-168. https://doi.org/10.1109/TPAMI.1980.4766994.

[53] Carreño Conde, F. and De Mata Muñoz, M., (2019). Flood Monitoring Based on the Study of Sentinel-1 SAR Images: The Ebro River Case Study. *Water*, Vol. 11(12). https://doi.org/10.3390/w11122454.

[54] Bioresita, F., Puissant, A., Stumpf, A. and Malet, J. P., (2019). Fusion of Sentinel-1 and Sentinel-2 Image Time Series for Permanent and Temporary Surface Water Mapping. *International Journal of Remote Sensing*, Vol. 40(23), 9026-9049. https://doi.org/10.1080/01431161.2019.1624869.

[55] Martinis, S., (2017). Improving Flood Mapping in Arid Areas Using Sentinel-1 Time Series Data. *IEEE International Geoscience and Remote Sensing Symposium (IGARSS)*. 193-196. https://doi.org/10.1109/IGARSS.2017.8126927.

[56] Jarrett, S. and Hölbling, D., (2023). Spatial Evaluation of a Natural Flood Management Project Using SAR Change Detection. *Water*, Vol. 15(12). https://doi.org/10.3390/w15122182.

[57] Martinis, S., Groth, S., Wieland, M., Rättich, M. and Knopp, L., (2022). Improving Reliability in Flood Mapping by Generating a Global Seasonal Reference Water Mask Using Sentinel-1/2 Time-Series Data. *The International Archives of the Photogrammetry, Remote Sensing and Spatial Information Sciences*, 1127-1132. https://doi.org/10.5194/isprs-archives-XLIII-B3-2022-1127-2022.

[58] Jensen, J. R., (2005). *Introductory Image Processing: A Remote Sensing Perspective*. Upper Saddle River: Pearson Prentice-Hall.

[59] Fitzpatrick-Lins, K., (1981). Comparison of Sampling Procedures and Data Analysis for Land Use and Land Cover Maps. *Photogrammetric Engineering & Remote Sensing*, Vol. 47(3), 343-351.

[60] Enhancing Climate Resilience in Thailand Through Effective Water Management and Sustainable Agriculture. Green Climate Fund. [Online]. Available: https://www.undp.org/sites/g/files/zskgke326/files/migration/th/UNDP_TH_ESMF_ENG.pdf. [Accessed: Sep. 11, 2024].

[61] Congalton, R. G. and Green, K., (2019). *Assessing the Accuracy of Remotely Sensed Data: Principles and Practices*. 3rd ed. Boca Raton: CRC Press.

[62] Landis, J. R. and Koch, G. G., (1977). The Measurement of Observer Agreement for Categorical Data. *Biometrics*, Vol. 33(1), 159-174.

[63] Bioresita, F., Puissant, A., Stumpf, A. and Malet, J. P., (2019). Fusion of Sentinel-1 and Sentinel-2 Image Time Series for Permanent and Temporary Surface Water Mapping. *International Journal of Remote Sensing*, Vol. 40(23); 9026-9049. https://doi.org/10.1080/01431161.2019.1624869.

[64] Conversi, S., Carrion, D., Norcini, A. and Riva, M., (2023). Integrating Optical and Radar Imagery to Enhance River Drought Monitoring. *International Archives of the Photogrammetry, Remote Sensing and Spatial Information Sciences*, Vol. 48(1), 1363-1371.

[65] Wu, H., Song, H., Huang, J., Zhong, H., Zhan, R., Teng, X., Qiu, Z., He, M. and Cao, J., (2022). Flood Detection in Dual-Polarization SAR Images Based on Multi-Scale Deeplab Model. *Remote Sensing*, Vol. 14(20). https://doi.org/10.3390/rs14205181.

[66] Mansourpour, M., Rajabi, M. A. and Blais, J. A. R., (2006). Effects and Performance of Speckle Noise Reduction Filters on Active Radar and SAR Images. *International Society for Photogrammetry and Remote Sensing (ISPRS)*, Vol. 36(1). https://www.isprs.org/proceedings/xxxvi/1-W41/makaleler/Rajabi_Specle_Noise.pdf.

[67] Lee, J. S., Wen, J. H., Ainsworth, T. L., Chen, K. S. and Chen, A. J., (2008). Improved Sigma Filter for Speckle Filtering of SAR Imagery. *IEEE Transactions on Geoscience and Remote Sensing*, Vol. 47(1), 202-213. https://doi.org/10.1109/TGRS.2008.2002881.

[68] Sun, Z., Zhang, Z., Chen, Y., Liu, S. and Song, Y., (2019). Frost Filtering Algorithm of SAR Images with Adaptive Windowing and Adaptive Tuning Factor. *IEEE Geoscience and Remote Sensing Letters*, Vol. 17(6), 1097-1101. https://doi.org/10.1109/LGRS.2019.2939208.